



OPEN Design, synthesis and pharmacological evaluation of 1,4-naphthoquinone- 1,2,3-triazole hybrids as new anticancer agents with multi-kinase inhibitory activity

Pegah Mardaneh^{1,2,4}, Somayeh Pirhadi², Maryam Mohabbati², Mehdi Khoshneviszadeh², Zahra Rezaei¹, Luciano Saso³, Najmeh Edraki²✉ & Omidreza Firuzi²✉

Targeting important oncogenic kinases that contribute to hallmarks of cancer has revolutionized cancer therapy. Ten 1,4-naphthoquinone derivatives linked to 1,2,3-triazole (4a-4j) were designed and synthesized as kinase inhibitors especially aimed at blocking CDK2, a validated and important cancer target. Assessment of the antiproliferative activity of the synthesized compounds against lung (EBC-1), pancreatic ductal adenocarcinoma (PDAC, AsPC-1 and Mia-Paca-2), colorectal (HT-29), and breast cancer (MCF-7) cells revealed that most of the derivatives possess considerable antiproliferative potential, with IC_{50} values as low as 0.3 μ M. In contrast, the compounds relatively spared NIH3T3 non-cancer cell line. The kinase inhibitory effect of the best compounds was examined against a panel of 30 important oncogenic kinases. Derivatives 4a (bearing a benzyl ring) and 4i (bearing a *p*-methyl benzyl ring) inhibited CDK2, FLT4 (VEGFR3) and PDGFRA kinases with IC_{50} values in the range of 0.55–1.67 and 0.22–11.32 μ M, respectively. These compounds also caused S phase arrest and induced characteristic features of apoptosis in PDAC cells. Molecular modeling simulation validated the binding interactions between the synthesized derivatives and the active sites of the 3 target kinases. Finally, the compounds also possessed drug-like features as examined by *in silico* studies. The results of this study indicate that 1,4-naphthoquinone derivatives could have promising anticancer potential as multi-kinase inhibitors.

Keywords 1,4-Naphthoquinone derivatives, Targeted therapy, CDK2 inhibitor, Antitumoral agents, Drug design

Abbreviations

CDK	cyclin-dependent kinase
FDA	Food and Drug Administration
MD	molecular dynamic
PDGFRA	platelet-derived growth factor receptor
RMSD	root-mean-square deviation
RMSF	root-means-square fluctuation
RTK	receptor tyrosine kinases
TEA	triethylamine
TLC	thin layer chromatography

¹Department of Medicinal Chemistry, School of Pharmacy, Shiraz University of Medical Sciences, Shiraz, Iran.

²Medicinal and Natural Products Chemistry Research Center, Shiraz University of Medical Sciences, Shiraz, Iran.

³Department of Physiology and Pharmacology Vittorio Erspamer, Sapienza University of Rome, P. le Aldo Moro 5, Rome 00185, Italy. ⁴Student Research Committee, Shiraz University of medical Sciences, Shiraz, Iran. ✉email: edrakin@sums.ac.ir; firuzio@sums.ac.ir

VEGFR-3 vascular endothelial growth factor receptor-3

The world faced approximately 19.3 million newly diagnosed cases of cancer in 2020 and this number is projected to increase to 28.4 million by 2040¹. Furthermore, cancer is the first or the second most common cause of death in 112 out of 183 countries². These frightening numbers are largely due to the fact that currently available therapeutic options often fail in the advanced stages of many types of cancer. Hence, exploring new targeted therapies designed to specifically suppress main oncogenic pathways in cancer cells is of crucial importance^{3,4}.

Protein kinases include important families such as serine/threonine kinases and receptor tyrosine kinases (RTK), and by phosphorylating nearly 30% of proteins in cells, play important roles in regulating important signaling pathways involved in different hallmarks of cancer including proliferation, invasion, angiogenesis among others^{5,6}.

It has been suggested that simultaneous inhibition of several kinases may provide the opportunity to suppress multiple pathways of cancer at the same time, and hence be more effective than modulation of a single target. This approach may offer some advantages such as improved efficacy, prevention of pharmacokinetic incompatibilities, and reduced toxicity⁷. The Food and Drug Administration (FDA) has given approval to several multiple kinase drugs that target enzymes involved in cancer growth for treating advanced stages of cancers.^{8–10} The general structure of multi-kinase inhibitor compounds is depicted in three parts, each highlighted in a different color. The main backbone, consisting of various heterocyclic rings (oxindole, pyridine, and pyrimidine) is colored in blue, while the hydrogen-bond interaction site (amide and urea group) and the hydrophobic tail are depicted in green and brown, respectively (Fig. 1).

The pharmacophoric features of sunitinib, a drug that targets several RTKs, demonstrate that its heterocyclic aromatic ring (oxindole ring), linker (pyrrole), hydrogen-bond donating/accepting interaction (amide group) and a hydrophobic tail (diethylamine group) are features that may enable the compound to fit into the active site of several kinases and act as a multi-kinase inhibitor¹¹. In sorafenib, another FDA-approved multi-kinase inhibitor, the diaryl-urea moiety in combination with aromatic heterocyclic rings (pyridine), may be involved in blocking several oncogenic kinases¹². Imatinib, another multi-kinase inhibitor approved for efficacious treatment of chronic myelogenous leukemia has a pyrimidine ring and amide linker that create extra hydrogen bond interactions with various targets¹³.

Among protein kinases, cyclin-dependent kinases (CDKs) are an important group of serine threonine kinases that are specifically involved in cell cycle regulation. Different types of cancer are linked to abnormal activation of CDKs¹⁴. The activation of CDK2 resulting from its binding with cyclin E or cyclin A regulates cell cycle progression during G1 and S phases^{15–17}. Recently, structures containing fused pyrimidine rings such as seliciclib (roscovitine), dinaciclib and BS-194 have been found to possess potent CDK2 inhibitory activity and anticancer potential^{18–20}. El-Moghazy and colleagues synthesized a fused pyrimidine structure, identified through molecular modeling, as a potent and selective CDK2/cyclin A kinase inhibitor (compound I, Fig. 2), exhibiting an IC_{50} value of 0.05 μ M and considerable growth inhibition against non-small cell lung cancer²¹. Another compound K03861, has demonstrated potent CDK2 inhibition with a K_d of 8.2 nM²². In their efforts to develop CDK2 inhibitors for treating breast cancer, Wang and colleagues designed new pyrimidine derivatives (compound II) exhibiting potent and selective enzymatic activity against CDK2, with an IC_{50} value of 54.3 nM²³. Pyrimidine cores originating from a commercially available kinase-directed library were also found to be highly potent CDK2 inhibitors²⁴. The key structural features of these entities are similar to multi kinase inhibitors including hetero-aromatic rings (colored blue) connected through the hetero atom containing linker to hydrogen bond accepting/donating nitrogen bearing moiety (colored green) with aromatic tail ended pendant (colored brown).

On the other hand, the anticancer activity of 1,4-naphthoquinone derivatives, both synthetic and natural, has been reported^{25–27} (Fig. 2). In particular, several 1,4-naphthoquinone derivatives, such as doxorubicin, daunorubicin, and mitoxantrone, have been used as efficacious anticancer agents for several decades^{28–30}. Previously, we synthesized 1,4-naphthoquinone containing 1,2,3-triazole moiety (compound VI, Fig. 2) demonstrating high antiproliferative activity against several cancer cell lines³¹.

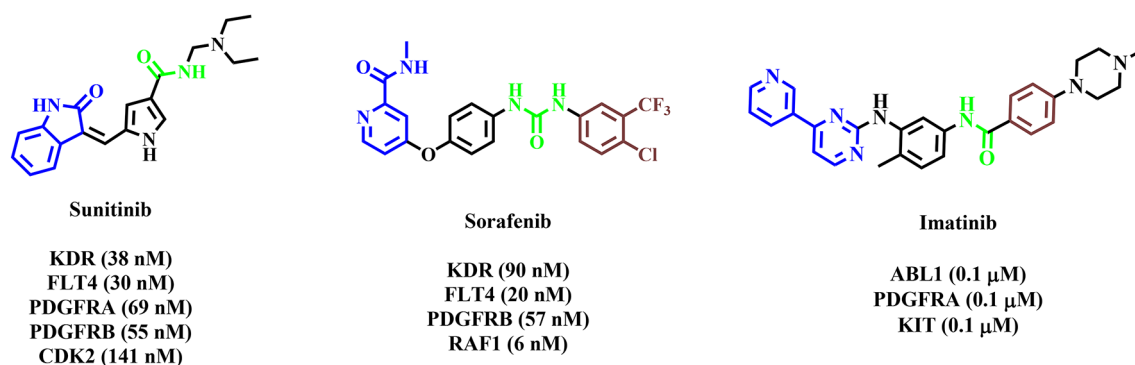


Fig. 1. Chemical structures and key structural features of FDA-approved multi-kinase inhibitors. The IC_{50} value for each kinase is shown in parentheses^{8–10}. The main backbone is colored in blue, while the hydrogen-bond interaction site and the hydrophobic tail are depicted in green and brown, respectively.

Another important moiety that confers anticancer potential is the 1,2,3-triazole group, which has distinctive features in medicinal chemistry³² (Fig. 2). The structure similarity of 1,2,3-triazole to amide bonds (colored green), particularly with regard to distance and planarity further enhances its unique properties in medicinal chemistry for developing the library of compounds for investigation of structure-activity relationship. Many investigators have reported the anticancer potential of 1,4-naphthoquinone derivatives connected to a 1,2,3-triazole group against colon, breast, lung and prostate cancers as well as acute lymphoblastic leukemia (Fig. 2)^{33–35}. Compounds **III**, **IV**, and **V**, which contain a 1,2,3-triazole moiety hybridized with a 1,4-naphthoquinone ring, have demonstrated enhanced anti-proliferative activities against cancer cell lines^{36–38} (Fig. 2).

Inspired by these findings, we designed novel multi-kinase inhibitors targeting CDK2 in which heteroaromatic group of multi kinase and CDK2 inhibitors were isosterically replaced by 1,4-naphthoquinone (colored red) moiety to improve antiproliferative effect and binding affinity to optimize potency for tumor cell growth inhibition. Furthermore, in attempt to enhance the potency of designed scaffold, 1,2,3-triazole ring was used in place of amide, urea, or thiourea groups of CDK2 and multi-kinase inhibitors to design novel 1,4-naphthoquinones derivatives connected via phenoxy linker to 1,2,3-triazole moieties bearing different substituted aryl pendants. It is obvious that from one side the general backbone and key fragments of multi-kinase inhibitors (Fig. 1) have been preserved in the designed scaffold and from the other side it could mimic the structural features of CDK2 inhibitors (Fig. 2). The key structural pharmacophoric fragments are appropriately colored in the structures. The kinase inhibitory effect of these candidates was examined and their ability to suppress cell growth was evaluated in cell culture models. Finally, in order to analyze the binding mode of target compounds and their interactions with target kinases, we performed molecular docking and molecular dynamic simulation.

Results

Synthesis

Figure 3 illustrates the step-by-step process for the synthetic pathway of new compounds.

Initially, we prepared 1-nitro-4-(prop-2-yn-1-yloxy) benzene (**1**) via the reaction of 4-nitrophenol and propargyl bromide under reflux condition in the presence of K_2CO_3 in acetone. In the second step, various intermediate compounds (**2a–j**) were produced by reacting different substituted benzyl halide and isoindoline derivatives with sodium azide in the presence of triethylamine (TEA) in *t*-BuOH/ H_2O (4:1) solvent system at 70 °C for 30 min. Subsequently, intermediate compound (**1**) was added to the reaction mixture with catalytic amount of $CuSO_4 \cdot 5H_2O$ (10 mol%) and sodium ascorbate, maintaining the temperature at 40 °C. Once the reaction was complete, the mixture was purified by thin layer chromatography (TLC) in EtOAc/*n*-hexane (4:6). Raney Nickel reduced the nitro group at 60 °C in the third stage to afford amine compounds (**3a–j**). Finally, in order to obtain target compounds **4a–j**, 1,4-naphthoquinone was completely dissolved in hot ethanol and the intermediates (**3a–j**) were slowly added at room temperature. Final products were recrystallized from appropriate solvent and characterized by different spectroscopic assays. The chemical structure, and physiochemical properties of all synthetic compounds are demonstrated in Table 1.

Antiproliferative effect against cancer cells

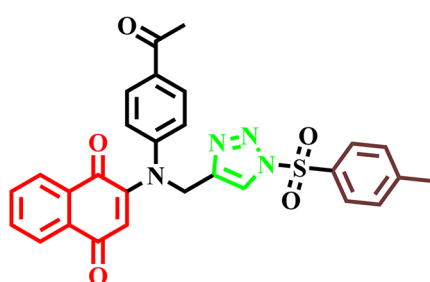
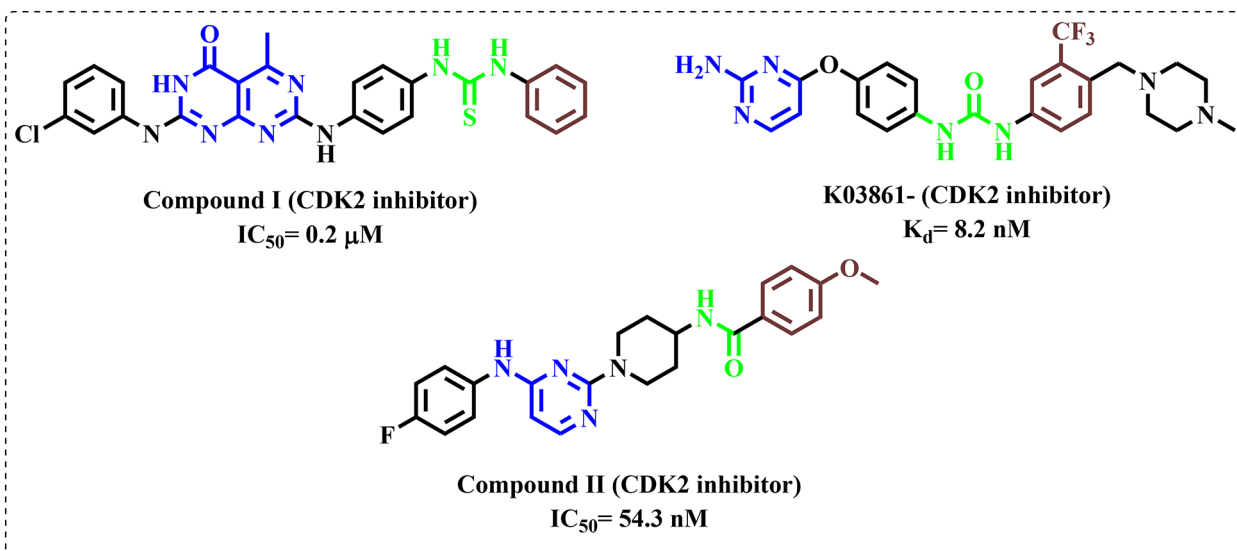
Five different cancer cell lines were used to evaluate the antiproliferative activity of the new series of 1,4-naphthoquinone derivatives: lung (EBC-1), PDAC (AsPC-1, Mia-Paca-2), colorectal (HT-29) and breast cancer (MCF-7) cells using the MTT reduction assay. The calculated IC_{50} values of all synthetic compounds as well as doxorubicin, cisplatin and cabozantinib tested as references drugs, are reported in Table 2. All compounds, except for **4j**, demonstrated moderate to high level of antiproliferative activity when tested against various cancer cell lines. Derivatives **4a**, **4b**, **4d**, **4e**, **4f**, **4g**, and **4i** overall exhibited highest antiproliferative effects against cancer cells. Compounds **4b**, **4d**, **4e** and **4g** were the most effective derivatives against EBC-1 cells with IC_{50} values of 2.0, 1.9, 0.3 and 2.0 μM , respectively. The most potent compounds against AsPC-1 cell line were **4e** and **4i**, which suppressed cancer cell viability with low IC_{50} values of 1.1 and 5.4 μM , respectively. Compounds **4b** and **4e** showed high antiproliferative effects against Mia-Paca-2 PDAC cells with IC_{50} values of 1.3 and 0.8 μM , respectively. Additionally, **4e** and **4i** compounds were both the best compounds against HT-29 and MCF-7 cells with IC_{50} values ranging from 0.6 to 13.9 μM . Considering these findings, compounds **4a**, **4b**, **4e**, **4g**, and **4i** were selected for measurement of activity against a panel of oncogenic kinases. Moreover, the toxicity of synthetic compounds was also assessed against NIH3T3 non-cancer cell line, to make comparisons with their effect against cancer cells. The findings indicated that compound **4a** exhibits low toxicity against non-cancer cells (IC_{50} = 85.5 μM).

Kinase selectivity profile

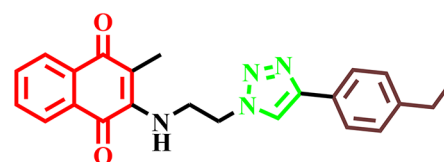
Five selected compounds (**4a**, **4b**, **4e**, **4g**, and **4i**) were tested for their inhibitory action against a panel of important human protein kinases. A radiometric assay was used for the initial screening, at a concentration of 10 μM . The results indicated that compounds **4a** and **4i** were capable of inhibition of three kinases including CDK2, FLT4 (VEGFR3), and PDGFRA at 51–87% (Table 3).

In the next step, we obtained the concentration-response curves of these two derivatives and calculated IC_{50} values against the three mentioned kinases. The results are shown in Fig. 4; Table 4. We found that compounds **4a** and **4i** inhibit these kinases with low IC_{50} values ranging from 0.220 to 11.3 μM .

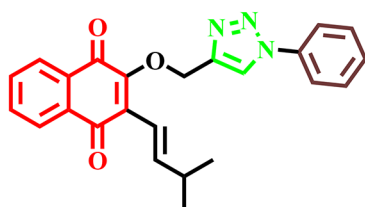
The values are shown as mean \pm S.D. Reported IC_{50} values for trilaciclib³⁹ (CDK2 inhibitor), vandetanib⁴⁰ (FLT4 inhibitor), and nintedanib⁴¹ (PDGFRA inhibitor) as reference compounds are 1.6, 110.0, and 59.0 nM respectively.



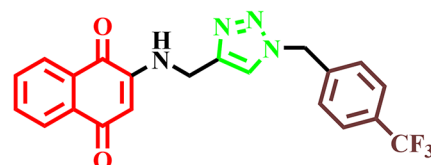
III
HCT-116 (0.6 μM)
MCF-7 (0.4 μM)
NCIH460 (0.5 μM)



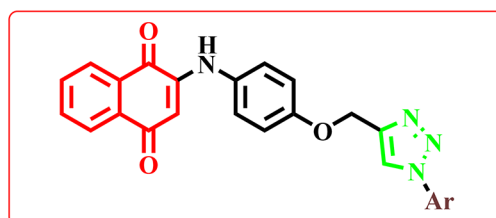
IV
A549 (9.1 μM)
MCF-7 (8.7 μM)
DU-145 (8.0 μM)



V
SCC-4 (28.8 μM)
SCC-9 (66.0 μM)
SCC-25 (9.8 μM)



VI
MCF-7 (10.4 μM)
HT-29 (6.8 μM)
MOLT-4 (8.4 μM)

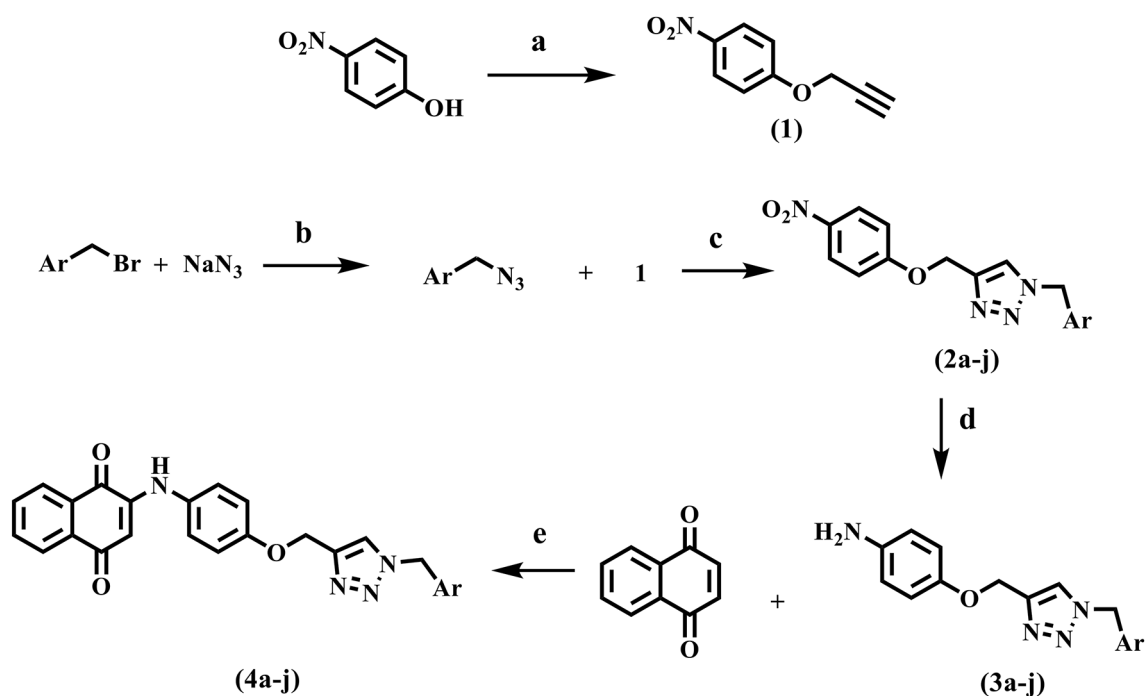


Designed scaffold

Cell cycle

To further examine the underlying mechanisms of anticancer effect of potent 1,4-naphthoquinone derivatives, we conducted cell cycle study of AsPC-1 cells treated with compounds **4a**, **4e**, and **4i** at 3, 10, 30, 50 μM using RNase/PI assay. Derivatives **4a** and **4i** were chosen due to their interesting effects against 3 oncogenic kinases,

Fig. 2. Design strategy of 1,4 naphthoquinone – 1,2,3 triazole hybrid derivatives. 1,4 Naphthoquinone – 1,2,3-triazoles were designed as multi-kinase inhibitors inspired by previously reported multi-target inhibitors shown in Fig. 1, as well as CDK-2 inhibitors^{21–23} and antiproliferative agents^{31,36–38}. IC₅₀ values for antiproliferative effect against cell lines are reported in parenthesis. The key structures of CDK2 inhibitors (hetero-aromatic rings) is colored in blue, while the hydrogen bond accepting/donating moieties and the aromatic ring are depicted in green and brown colors, respectively.



- | | |
|------------------------------------|---------------------------------------|
| 4a: Ar= Phenyl | 4f: Ar= 3-Cl-phenyl |
| 4b: Ar= 4-Br-phenyl | 4g: Ar= 4-i-Pr-phenyl |
| 4c: Ar= 4-F-phenyl | 4h: Ar= 4-t-Bu-phenyl |
| 4d: Ar= 4-Cl-phenyl | 4i: Ar= 4-Me-phenyl |
| 4e: Ar= 3,4-Dichloro-phenyl | 4j: Ar= N-(2-Ethyl) phthalimid |

Fig. 3. Synthetic route of new 1,4 naphthoquinone derivatives. (a) Propargyl bromide, K₂CO₃, acetone, Reflux, 5 h. (b) TEA, t-ButOH/H₂O, 70 °C, 30 min. (c) CuSO₄·5H₂O (10 mol %) and Sodium ascorbate (25 mol%), at 40 °C, 48 h. (d) NH₂NH₂, H₂O, Raney Nickel, EtOH/H₂O, 60 °C, 15 min. (e) EtOH, RT.

while compound **4e** was selected because of its potent effects against all tested cancer cell lines. Figure 5 depicts characteristic histograms of the cell distributions in G0/G1, S, and G2/M phases.

We observed that all 3 compounds exhibited a dose-dependent effect, leading to an increase in the percentage of S phase cells and a corresponding decrease in cells in the G2/M phase of the cell cycle (Fig.s 5–6). In addition, compound **4e** specifically caused an increase in cells in sub-G1 phase, while reducing G0/G1 cells.

Apoptosis measurement by Hoechst 33,258 staining

Hoechst 33,258 staining was employed to distinguish apoptotic cell death in ASPC-1 cells that were treated with 1,4-naphthoquinone derivatives. Compounds **4a**, **4e**, and **4i** were exposed to the cells for 48 h at concentrations of 10 and 30 µM. The images showed a decreased cell density compared to the control, along with characteristic features of apoptosis including densely packed chromatin within the nucleus as well as nuclear fragmentation (Fig. 7). Therefore, it can be assumed that these compounds possess the ability to induce apoptosis in cancer cells.

Computational study Molecular Modelling Study

Molecular docking study of compound 4a with CDK2, FLT4, and PDGFRA proteins

In order to evaluate the specific interaction patterns and binding configurations of synthetic compounds within the active site of CDK2, FLT4, and PDGFRA kinases, selected 1,4-naphthoquinone derivatives were

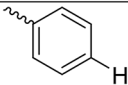
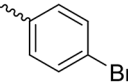
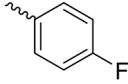
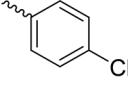
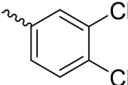
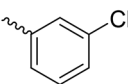
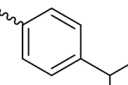
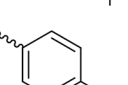
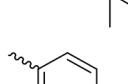
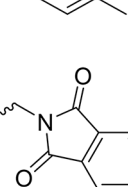
Compound	Ar	m.p. (°C)	Yield (%)
4a		177-179	93
4b		172-174	96
4c		190-192	94
4d		164-166	92
4e		179-181	82
4f		168-170	87
4g		182-185	78
4h		212-215	76
4i		187-191	79
4j		254-257	62

Table 1. The chemical structures and physical properties of the novel 1,4 naphthoquinone derivatives.

computationally fitted into the active site of three kinase targets using the smina docking tool. The docking analysis utilized the crystal structure of CDK2 bound with cyclin A (PDB code: 4BCQ), and PDGFRA (PDB code: 6JOL). Due to the lack of an experimental structure, the predicted 3D structure of FLT4 was downloaded from the AlphaFold database (<https://alphafold.ebi.ac.uk>)⁴² (UniProt code: P35916). The root-mean-square deviation (RMSD) values of the re-docking of native ligands TJF and imatinib were 1.62 and 1.48 Å within the active site of CDK2/ cyclin A and PDGFRA receptors, respectively, which are lower than the tolerable marginal value of 2 Å. The superimposition of the native ligands on the docked poses is shown in Fig. 8.

The docking interactions and minimized affinities of CDK2/cyclin A receptor are predicted in the **Supplementary Table 1 S**. The minimized affinity of the native ligand TJF for the CDK2/cyclin A target was determined to be −7.40 kJ/mol, with hydrogen bond interactions observed with key residues Asp86 and Leu83, as well as π -anion interactions with residue Asp145. Furthermore, π -alkyl interactions were observed with residues Ile10, Leu134, and Val18, along with various Van der Waals interactions (see Fig. 9A). Compound **4a** exhibited the most promising potency, with a lower minimized affinity (−9.9 kcal/mol) and favorable interactions with the CDK2 (Fig. 9B). The carbonyl group of the 1,4-naphthoquinone ring and the NH group of compound **4a** participated in hydrogen bond interactions with Asp86 and Leu83, similar to the native ligand. The triazole ring displayed π - π T-shaped and π -sigma interactions with residues Phe80 and Ala144, respectively. The phenoxy ring created a π - π stacked interaction with Phe82. Furthermore, the phenoxy ring and benzyl ring of compound **4a** exhibited π -alkyl interactions with Ala31 and Leu134, respectively, Van der Waals interactions were identified as contributing to the binding mode of compound **4a** to the enzyme (Fig. 9B). Imatinib served as the native ligand of the PDGFRA receptor with a minimized affinity of −10.30 (kJ/mol) and binding interactions

Compound	EBC-1	AsPC-1	Mia-Paca-2	HT-29	MCF-7	NIH3T3
	IC ₅₀ (μM)					
4a	5.1 ± 1.2 bc	23.5 ± 5.8 fg	> 100	21.9 ± 3.9 b	> 100	85.5 ± 19.6 (1.7)* f
4b	2.0 ± 1.2 ab	30.7 ± 2.2 gh	1.3 ± 0.4 a	56.9 ± 4.3 c	> 100	50.9 ± 8.8 (1.3) e
4c	13.7 ± 3.3 d	34.8 ± 15.3 h	61.0 ± 6.6 e	> 100	26.9 ± 0.2 e	20.1 ± 3.3 (0.4) abc
4d	1.9 ± 0.3 ab	20.8 ± 6.8 defg	21.3 ± 3.6 b	3.1 ± 0.4 a	15.9 ± 4.6 cd	14.4 ± 1.9 (1.1) abc
4e	0.3 ± 0.1 a	1.1 ± 0.2 a	0.8 ± 0.1 a	0.6 ± 0.2 a	7.1 ± 4.3 ab	6.5 ± 1.2 (3.2) ab
4f	2.3 ± 0.4 ab	10.5 ± 2.6 abcd	42.1 ± 12.6 cde	1.9 ± 0.4 a	> 100	29.8 ± 7.3 (0.9) cd
4g	2.0 ± 0.5 ab	12.8 ± 2.9 bcde	45.0 ± 8.2 de	4.9 ± 0.9 a	22.3 ± 3.8 de	24.5 ± 5.2 (1.4) abcd
4h	8.7 ± 1.3 c	16.2 ± 2.0 cdef	31.3 ± 3.3 bcd	2.5 ± 0.7 a	20.3 ± 0.2 cde	46.7 ± 3.2 (2.9) de
4i	2.5 ± 0.3 ab	5.4 ± 0.9 ab	20.6 ± 6.2 b	1.3 ± 0.5 a	13.9 ± 0.7 bc	25.5 ± 6.1 (2.9) bcd
4j	> 50	> 100	> 100	> 50	> 100	n.d.
Doxorubicin	0.5 ± 0.1 a	1.73 ± 0.2 a	88.1 ± 52.6 [#] a	0.6 ± 0.2 a	137.0 ± 6.3 [#] a	13.0 ± 2.1 (0.02) [#] a
Cisplatin	24.0 ± 5.5 e	5.4 ± 0.6 ab	22.1 ± 6.2 abc	43.3 ± 17.3 c	43.1 ± 1.9 f	8.3 ± 1.4 (0.3) abc
Cabozantinib	0.06 ± 0.010 a	21.28 ± 2.03 efg	7.4 ± 0.6 ab	3.7 ± 0.4 a	17.8 ± 2.4 cd	n.d.

Table 2. Antiproliferative effects of the designed compounds (4a-i) evaluated against cancer cell lines by MTT test. The results are shown as mean ± S.E.M. of 3–5 independent experiments. Values within a column labeled with no common letters (e.g., a, b, c, etc.) indicate significant differences at $P < 0.05$. * Selectivity index (SI) values (shown in parentheses) were calculated as the ratio of the IC₅₀ value for NIH3T3 cells to the mean of the IC₅₀ values of all cancer cell lines. The IC₅₀ value for inactive compounds was assumed as 100 μM. [#] Results are expressed in nM. n.d.: Not determined.

including hydrogen bond interactions with Asp836, Glu644, Met648, Thr674, and Cys677; π - π stacked with Tyr676; π - π T-shaped with Phe837; π - σ with Val607, Thr674, and Leu599; π -cation with Lys627; π -alkyl with Cys677, Ile672, Met648, Ala625, and Leu825; and various van der Waals interactions (see Fig. 9C). Prediction of the binding mode and minimized affinity of selected 1,4-naphthoquinone derivatives with the PDGFRA kinase target is presented in **Supplementary Table 3 S**. The potent compound **4a**, formed two hydrogen bonds involving the carbonyl group of the 1,4-naphthoquinone ring, the oxygen group, and the nitrogen of the triazole ring with Cys677 and Asp836. Additionally, the phenyl group of the 1,4-naphthoquinone ring participates in π - π stacking interaction with Tyr676 residue, while the phenoxy ring maintained a π - π T-shaped interaction with Phe837. The 1,4-naphthoquinone ring and benzyl ring illustrated π -sigma interactions with Leu599, Leu825, and Ile647 residues. π -Anion and π -sulfur interactions were observed between the benzyl and triazole rings with Asp836 and Met648, respectively. Moreover, the 1,4-naphthoquinone ring and phenoxy ring formed π -alkyl interactions with Ala625, Val607, Val658, and Cys835, and exhibited seven Van der Waals interactions (see Fig. 9D). The results suggest that compound **4a** reaches the back hydrophobic pocket of the PDGFRA similar to imatinib. Selected compounds were also docked into the FLT4 protein, and the results of minimized affinities and binding interactions are represented in Supplementary Table 2 S. Regarding the literature, the majority of variants associated with causing lymphangiogenesis are found within the domain 845–1173 responsible for tyrosine kinase catalytic activity⁴³. The potent compound **4a** showed the best minimized affinity of −9.89 (kJ/mol) and hydrogen bond interaction between the carbonyl of the 1,4-naphthoquinone ring, the NH group, and the nitrogen of the triazole ring with Cys1054, Asn934, Arg1041, and Ser1275. Furthermore, π -sigma interaction can be seen between the 1,4-naphthoquinone ring and benzyl ring through Leu1044, Leu1058, and Ala855 residues. Additionally, Leu851, Val859, Cys1054, and Arg1041 residues made π -alkyl interactions with the 1,4-naphthoquinone ring and phenoxy ring. (See Fig. 9E).

Molecular dynamic simulation of compound 4a

Molecular dynamics (MD) simulations need to be run for an adequate duration to predict the accuracy of the binding interaction results. MD simulation of compound **4a** was performed with three targets: CDK2 bound with cyclin A, FLT4, and PDGFRA. The backbone root-mean-square deviation (RMSD) was computed to suggest the quantification of variations in atomic locations in simulation frames relative to a reference frame (Fig. 10A). The results revealed that the backbones of CDK2/cyclin A, FLT4, and PDGFRA remained relatively stable throughout the simulation period, with no significant changes. The radius of gyration (Rg) is a parameter used to estimate the root-mean-square distance of each amino acid atom from the protein's center, providing information about changes in compactness and flexibility within proteins. These complexes reached a plateau (Fig. 10B), indicating that the interaction with compound **4a** still preserves the stability and compactness of the protein. The RMSF plot of the backbone atoms of CDK2/cyclin A, FLT4, and PDGFRA targets were depicted in Fig. 10C and D, and 10E respectively. The RMSF results estimate the dynamic flexibility, vibration of amino acid residues, and influence on the stability of protein-ligand interactions throughout the MD period. This finding shows a low RMSF value and minimum alteration for the amino acids within the active sites of the three targets, suggesting a significant level of stability and preservation of the crucial residue interactions between the ligands and proteins. The key residues of the CDK2 complex did not show significant motions including Asp86, Leu83, and Phe82. The important binding site residues of FLT4 enzyme are Cys1054, Asn934, and Arg1041 which

Kinase name	Kinase inhibition (%)				
	4a	4b	4e	4 g	4i
1) ABL1	7	2	13	-	-
2) AKT1	19	9	15	-	-
3) AKT2	25	-10	-7	-	-
4) ALK	16	2	15	-	-
5) AURKA	-3	-	5	-	-
6) AXL	14	5	5	-	8
7) BRAF	3	-	-7	-	-
8) CDK2/cyclin A	73	32	9	1	51
9) CDK6/cyclinD3	9	-	3	-	-
10) CHEK1	-20	-	-12	-	-
11) EGFR	-5	-9	-3	-	-
12) ERBB2 (Her-2)	3	-	2	-	-
13) FGFR1	14	1	-5	-	-
14) FLT1 (VEGFR1)	-16	-17	-38	-	-17
15) FLT3	46	-3	-21	-2	-
16) FLT4 (VEGFR3)	87	26	30	9	87
17) IGF1R	-3	-	-11	-	-
18) KDR (VEGFR2)	20	-19	-9	-10	28
19) KIT (c-Kit)	1	-9	-8	-	-
20) MAPK1 (ERK2)	18	-	6	-	-
21) MAP2K1	9	-	4	-	-
22) MET	18	-8	-14	-11	16
23) NTRK1 (TrkA)	43	4	2	6	-
24) NTRK2 (TrkB)	0	13	6	-	19
25) NTRK3 (TrkC)	40	-	12	-	-
26) PDGFRA (PDGFR α)	71	37	43	29	74
27) PDGFRB (PDGFR β)	16	17	14	-	5
28) PIK3CA	14	-	3	-	-
29) ROS1	-6	-	-2	-	-
30) WEE1	6	-	-4	-	-

Table 3. Inhibitory effect of synthesized compounds 4a, 4b, 4e, 4 g, and 4i against a panel of critical kinases at 10 μ M concentration determined by a radiometric assay. The bold values depict kinase inhibition percentages exceeding 50%.

showed no significant fluctuation. The residues of the active site with lower fluctuation within the PDGFRA complex included Cys677, Asp836, and Tyr676.

The stability of complexes formed between ligands and proteins is greatly dependent on the hydrogen bond interactions. Therefore, the total hydrogen bond interaction between the three proteins (CDK2, FLT4, and PDGFRA) and compound **4a** is shown in Fig. 10F. The average number of hydrogen bonds observed for three complexes (CDK2, FLT4, PDGFRA proteins and compound **4a**) were 1.75, 2.09, and 0.72, respectively.

The cluster analysis of three complexes with compound **4a** was performed to identify the simulation's representative frames. The results estimated that 88.82% of the population was in cluster 3 with the CDK2/cyclin A complex, 98.14% in cluster 1 with FLT4, and 97.82% in cluster 2 with PDGFRA. Figure 11 displays the representative frames and the interaction patterns for each complex, and Fig. 83s (Supplementary Figures) displays the interaction pattern of representative frames of every cluster.

The complex of compound **4a** with CDK2 is shown in Fig. 11A. Carbonyl of 1,4-naphthoquinone ring and NH group formed hydrogen bond interaction with Gly12 and Asp85. Benzyl ring participated in π - π T-shaped interaction through Phe79 and the triazole ring made π -anion interaction with Asp144. Moreover, π -alkyl interaction with the 1,4-naphthoquinone ring, triazole ring, and benzyl ring by Ile11, Leu133, Ala30, Val17, and some Van der Waals interaction with the receptor can be seen.

Evaluation of the binding mode of compound **4a** with the FLT4 receptor is shown in Fig. 11B. The type of interaction with this receptor includes hydrogen bond interaction with 1,4-naphthoquinone ring and oxygen of phenoxy ring by Lys879 and Arg 1041, π -sigma interaction with 1,4-naphthoquinone ring through Val859, π -cation interaction with Arg940 by benzyl ring, π -alkyl interaction with 1,4-naphthoquinone ring through Leu1044, Val927, Ala877, Cys930, Val910, Cys1054, Arg1041 residues and some Van der Waals interaction with receptor.

Figure 11C shows that the complex of compound **4a** with the PDGFRA protein formed hydrogen bond interactions with the carbonyl group of the 1,4-naphthoquinone ring by Cys677 and Asp836 as key residues,

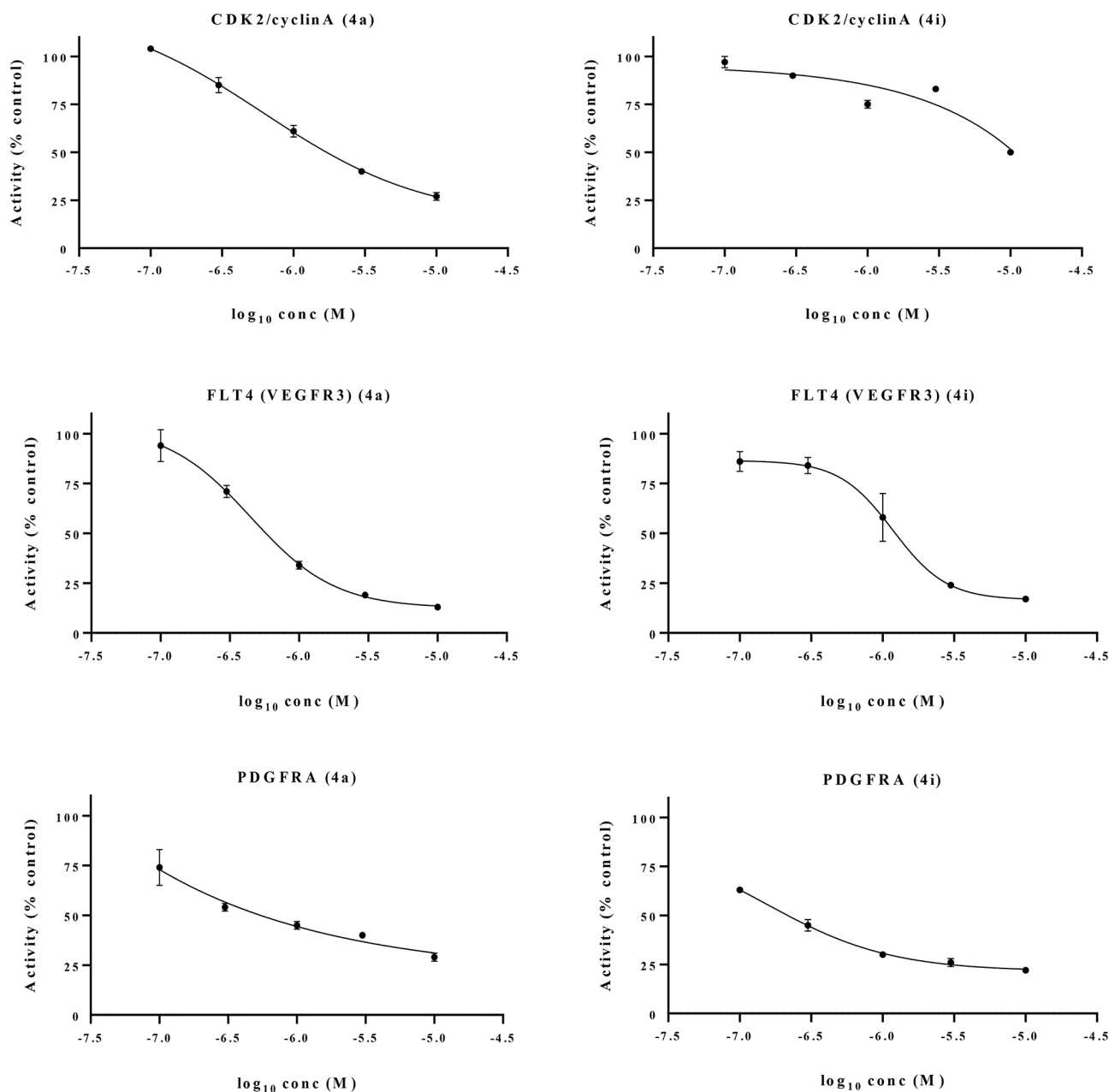


Fig. 4. Inhibitory activity of the compounds 4a and 4i against CDK2/cyclin A, FLT4 (VEGFR3), and PDGFRA kinases. A radiometric assay was carried out to measure the kinase inhibitory activity of the newly synthesized compounds.

	IC_{50} (μ M)		
Compound	CDK2/cyclin A	FLT4 (VEGFR3)	PDGFRA
4a	1.672 ± 0.115	0.554 ± 0.002	0.629 ± 0.087
4i	11.323 ± 0.477	1.336 ± 0.006	0.220 ± 0.009

Table 4. The inhibitory activity of compounds 4a and 4i against CDK2/cyclin A, FLT4 (VEGFR3), and PDGFRA kinases.

while a π -sigma interaction was detected between the 1,4-naphthoquinone ring and Leu599. Furthermore, the phenoxy ring participated in a π - π T-shaped interaction with Phe837, and an amide- π stacked interaction was noted with the benzyl ring through Cys835. Moreover, π -alkyl interactions occurred with Leu825, Ala625, Val 607, Lys627, Met648, Leu599, Cys677, and Cys835 involving the 1,4-naphthoquinone ring, phenoxy ring,

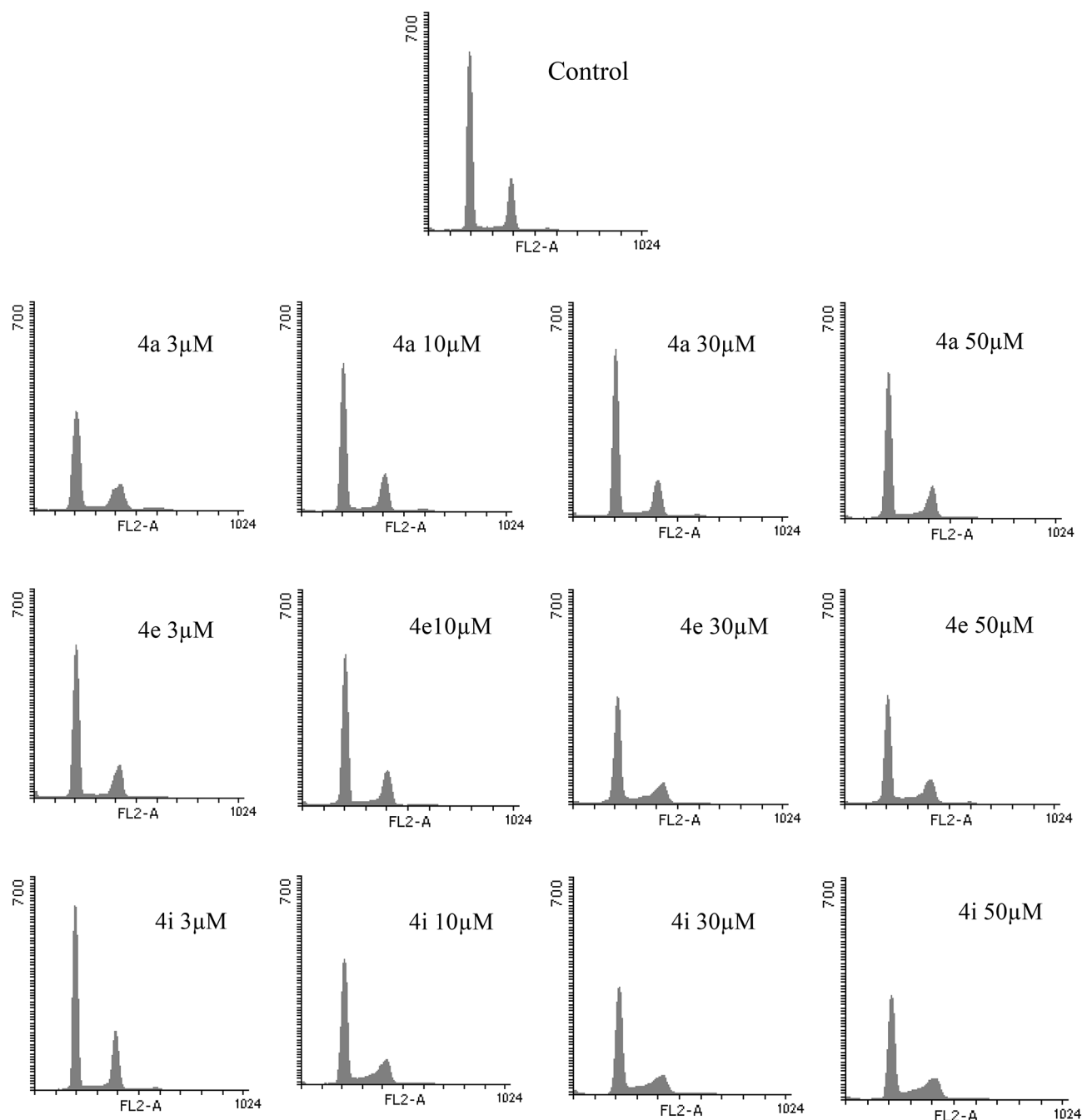


Fig. 5. Effect of 1,4-naphthoquinone derivatives on cancer cell cycle distribution. Select compounds at concentrations of 3, 10, 30, and 50 μM were added to AsPC-1 cells in 12-well microplates for a duration of 48 h. The cells were harvested in microtubes, rinsed with PBS, and subsequently fixed overnight at -20°C in 70% ethanol. The DNA staining solution, comprising propidium iodide (PI) at a concentration of $20\text{ }\mu\text{g/mL}$ and RNase at $200\text{ }\mu\text{g/mL}$, was applied to microtubes and incubated for 30 min in the dark at 37°C for subsequent analysis using a FACS Calibur flow cytometer (BD Biosciences). Representative histograms demonstrate the effect of **4a**, **4e**, and **4i** derivatives on AsPC-1 cell cycle distribution.

and triazole ring, along with some Van der Waals interactions with the receptor. The outcome suggested that compound **4a** interactions from MD simulations are in consistency with docking and shows good interaction with the pockets of three receptors.

Physicochemical parameters

The SwissADME online tool was used to analyze the physicochemical properties and drug-likeness of each targeted compound ⁴⁴. The comprehensive results in Table 5, show that most compounds comply with the criteria of Lipinski's rule of five, suggesting acceptable characteristics for potential oral bioavailability.

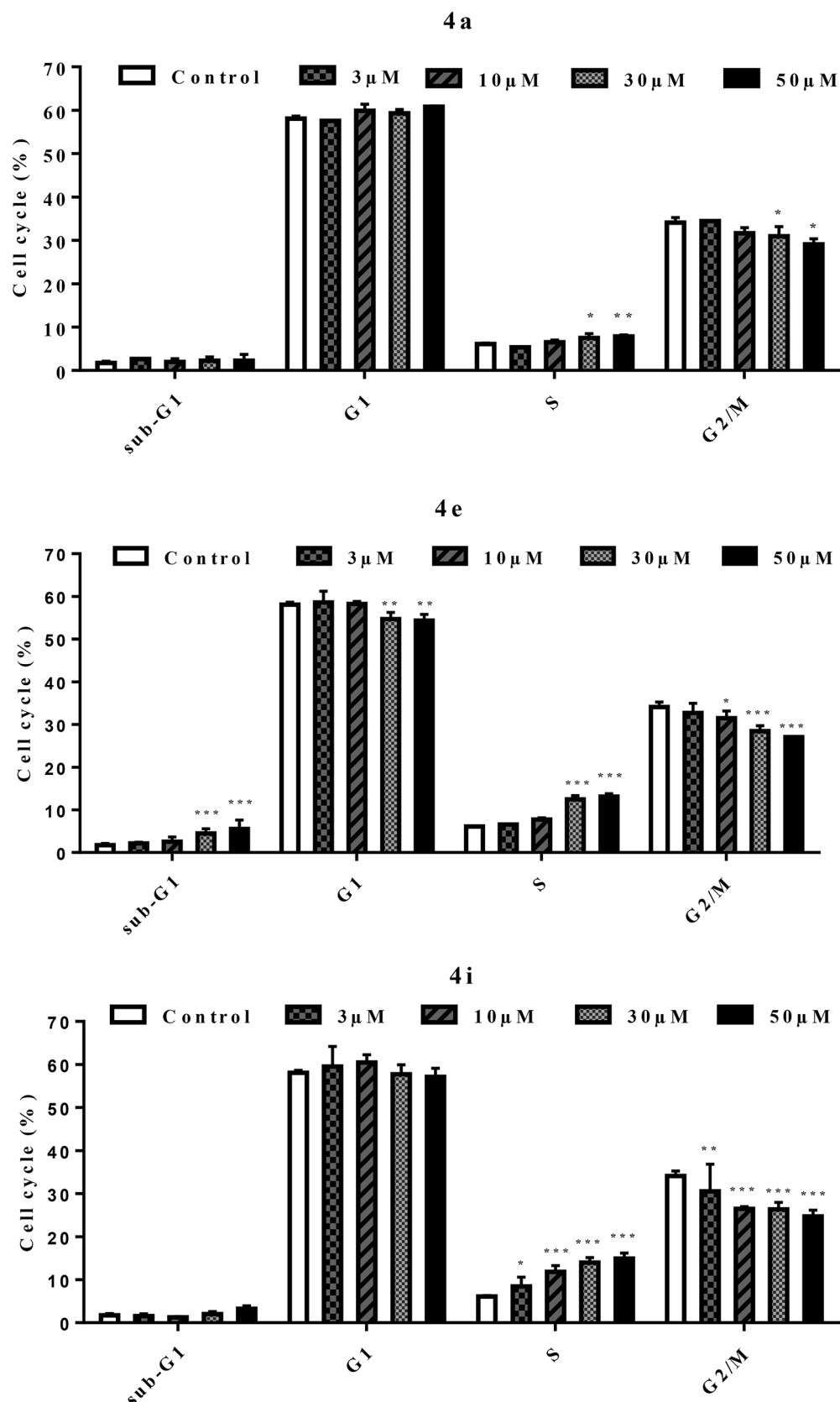


Fig. 6. Measurement of the effect of 1,4-naphthoquinone derivatives on cancer cell cycle distribution. Flow cytometry was utilized to analyze the cell cycle distribution in AsPC-1 cells in response to the compounds **4a**, **4e**, and **4i** at concentrations of 3, 10, 30, and 50 μ M, as described in the caption of Fig. 5. Statistical analysis revealed significant differences between the cells treated with the synthesized derivatives and the untreated control cells (*: $p < 0.05$, **: $p < 0.01$, ***: $p < 0.001$).

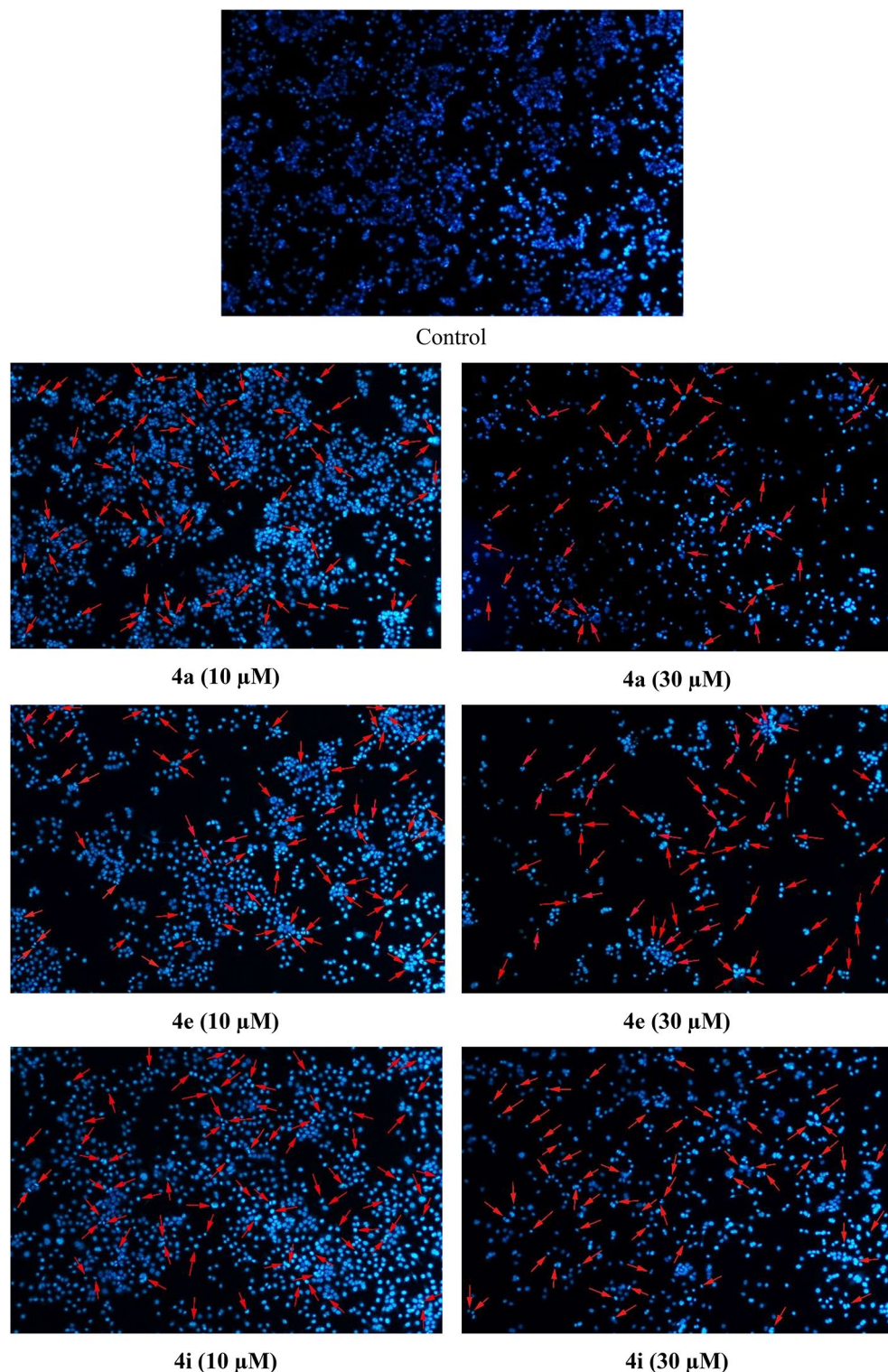


Fig. 7. Apoptosis induction in cancer cells by 1,4-naphthoquinone derivatives determined by Hoechst 33,258 staining. The synthesized compounds **4a**, **4e**, and **4i** were added to AsPC-1 cells in 6-well plates at 10 and 30 μM concentrations. After 48 h, each well was treated with 4% cold paraformaldehyde (PFA) to fix the cells, and 1 ml of Hoechst 33,258 at a concentration of 2.5 $\mu\text{g}/\text{ml}$. The images were captured using a fluorescence microscope. Red arrows show apoptotic cells.

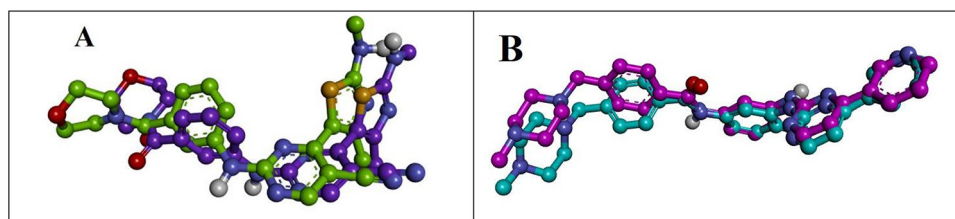


Fig. 8. TJF and imatinib in two different conformations in the active sites of CDK2/ cyclin A and PDGFRA. A: Crystal conformation and the re-docked model of TJF in the active site of CDK2/ cyclin A (PDB codes 4BCQ) are indicated by green and violet colors, respectively. B: Crystal conformation and the re-docked model of imatinib in the active site of PDGFRA (PDB code 6JOL) are indicated by purple and light blue colors, respectively.

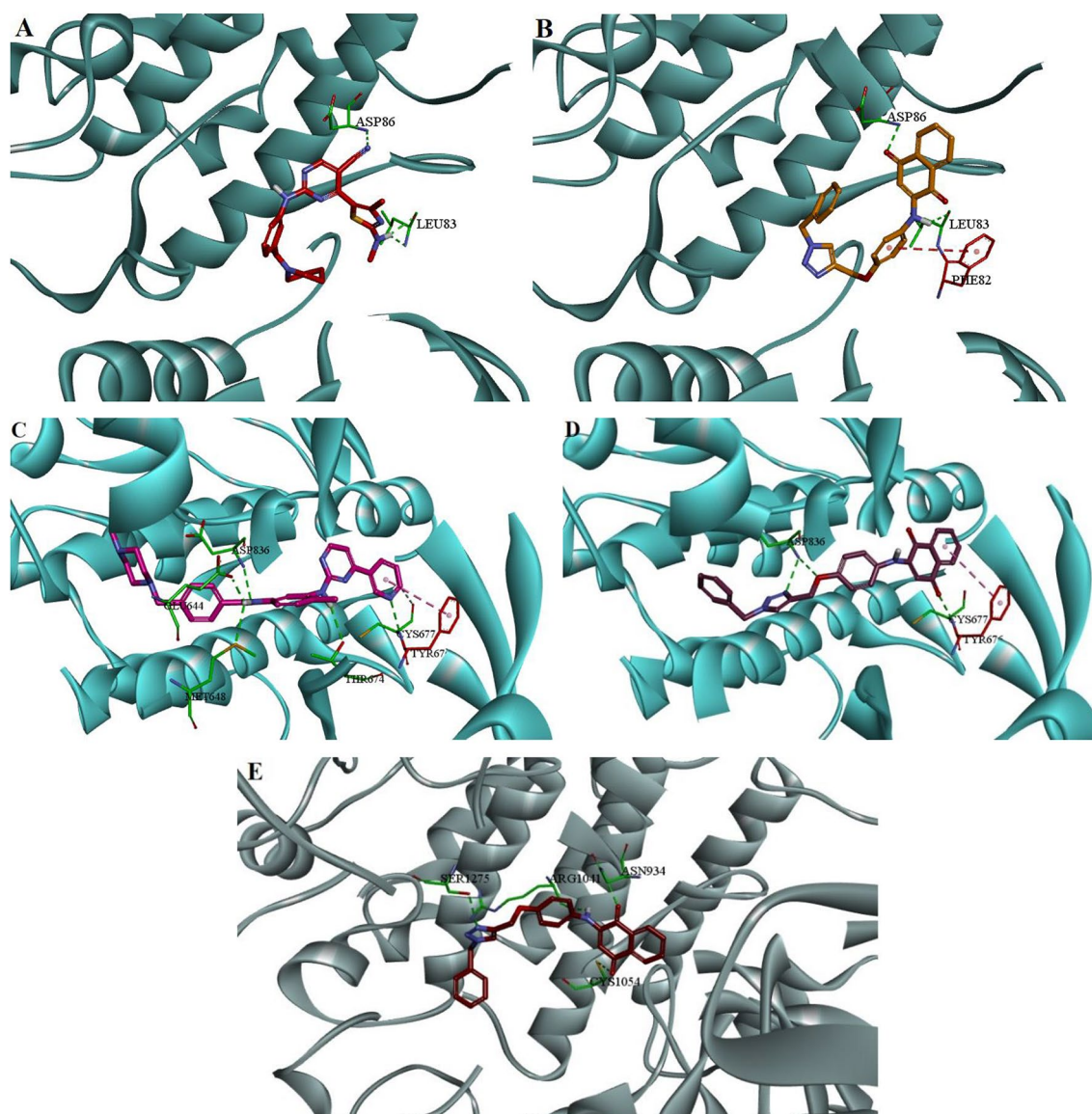


Fig. 9. 3D interaction of ligands with CDK2, PDGFRA, and FLT4 enzymes. A and B: binding interaction of TJF (native ligand) and **4a** derivative inside the CDK2 binding site, respectively. C and D: binding interaction of imatinib and compound **4a** inside the PDGFRA active site, respectively. E: binding interaction of **4a** derivative inside the FLT4 active site.

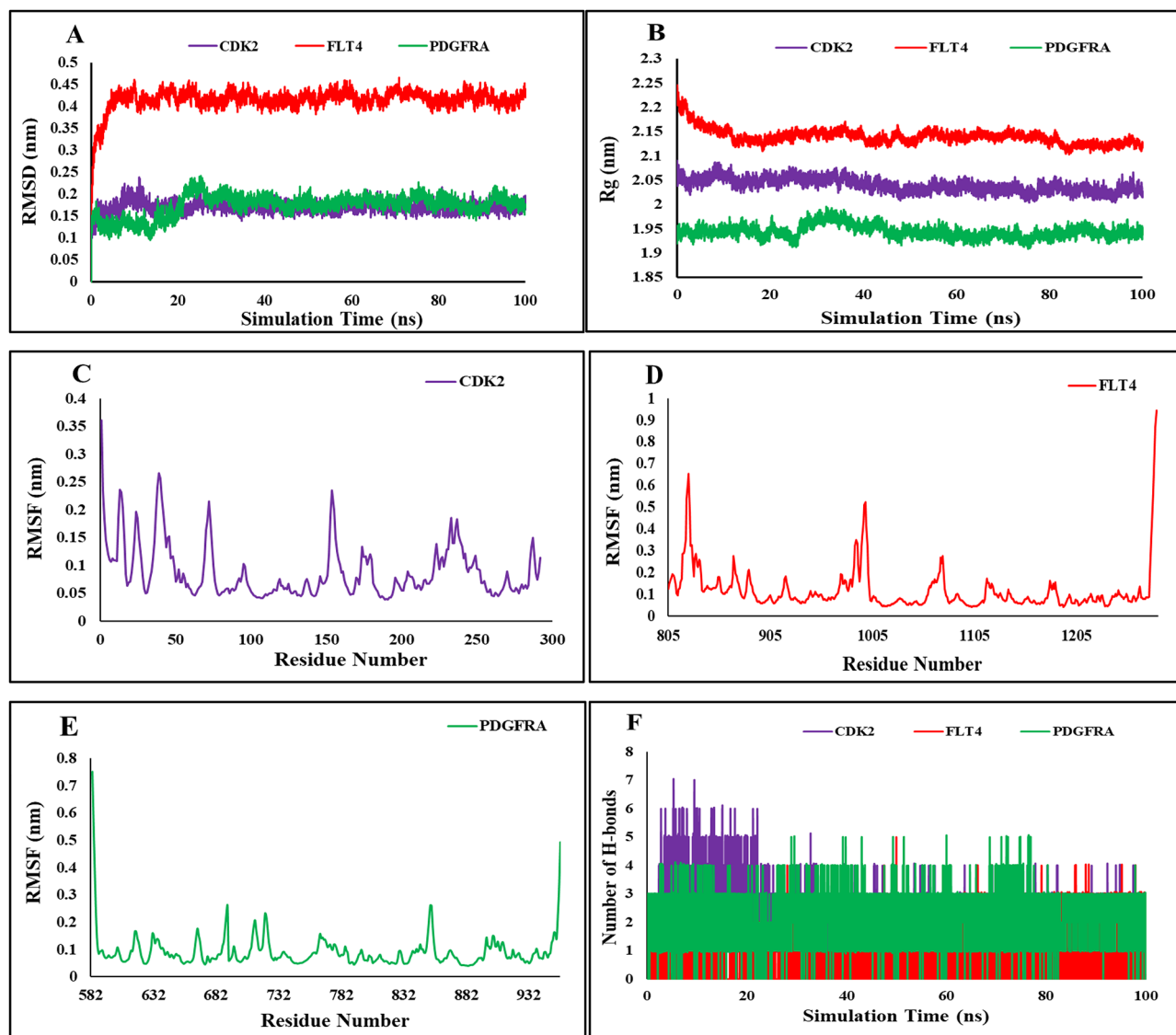


Fig. 10. Molecular dynamics analysis of compound 4a against CDK2, FLT4, and PDGFRA receptors. **A)** RMSD analysis of three complexes of CDK2/cyclin A, FLT4, and, PDGFRA targets over the simulation time, **B)** Rg analysis of three targets: CDK2/cyclin A, FLT4, and PDGFRA **C)** RMSF plot of CDK2/cyclin A target, **D)** RMSF plot of FLT4 target, **E)** RMSF plot of PDGFRA target, **F)** Total number of hydrogen bonds between CDK2/cyclin A, FLT4, and PDGFRA and compound 4a.

Discussion

A set of 10 1,4-naphthoquinone derivatives connected to triazole ring were synthesized and evaluated for the anticancer and kinase inhibitory potentials. The findings showed that the synthesized derivatives potently block the proliferation of several cancer cell lines and are promising inhibitors of 3 important oncogenic kinases, CDK2, FLT-4 (VEGFR3) and PDGFRA.

Following the design and synthesis of 1,4-naphthoquinone derivatives, we first examined their antiproliferative properties against five different types of cancer cells, including lung (EBC-1), PDAC (AsPC-1, Mia-Paca-2), colorectal (HT-29), and breast (MCF-7) cancers. Five derivatives among the synthesized compounds (**4a**, **4b**, **4e**, **4g**, and **4i**) demonstrated considerable anti-proliferative effects particularly against EBC-1 cells. Compound **4e** bearing 3,4 di-chloro benzyl pendant might be considered as promising candidate with encouraging antiproliferative potential with an IC_{50} range of 0.3 to 7.1 μ M against tested cell lines. While the presence of an unsubstituted benzyl pendant in **4a** conferred considerable antiproliferative effect against cancer cells, introduction of bulky electron withdrawing groups such as chlorine and bromine at para position of benzyl ring (**4b** and **4d**, respectively) resulted in superior antiproliferative effects. However, substitution of small electron withdrawing groups such as fluorine (compound **4c**) led to decreased overall activity. On the other hand, although compounds substituted with bulky lipophilic moieties such as, isopropyl (**4g**) and methyl (**4i**) showed considerable antiproliferative effect, t-butyl substitution (**4h**) decreased the potency. These observations indicate that the bulkiness of substituted moieties at para position of benzyl pendant should be optimized in

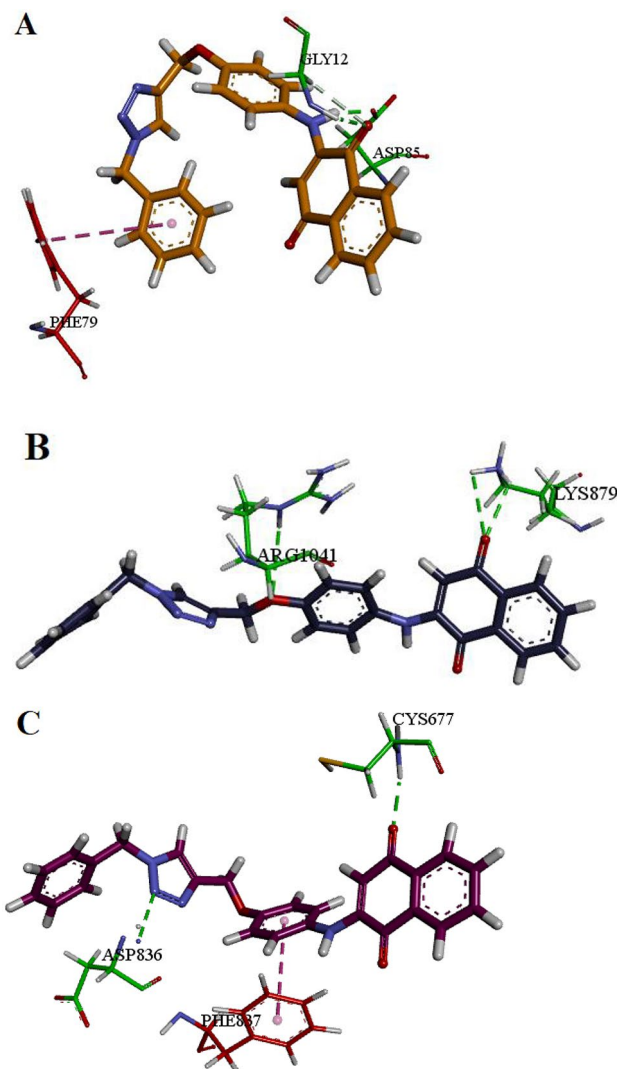


Fig. 11. 3D diagram of interaction of compound 4a with CDK2, FLT4, and PDGFRA proteins after MD simulation. Molecular dynamics simulation of the compound 4a with CDK2/cyclin A (A), FLT4 (B), and PDGFRA (C) enzymes. Hydrogen bonds and π - π T-shaped were colored as green and red.

Entry	MW (g/mol)	HBD	HBA	cLog <i>p</i>
4a	436.46	1	5	2.11
4b	515.36	1	5	2.68
4c	454.45	1	6	2.48
4d	470.91	1	5	2.58
4e	505.35	1	5	3.05
4f	470.91	1	5	2.58
4g	478.54	1	5	2.71
4h	492.57	1	5	2.90
4i	450.49	1	5	2.31
4j	519.51	1	7	1.99

Table 5. Physicochemical properties of the synthesized compounds.

order to produce favorable binding interactions with the molecular targets resulting in anticancer capacity. Moreover, it was observed that replacement of benzyl pendant with a bulky fused heterocycle such as indolinone as in compound 4j, rendered the compound devoid of any antiproliferative potential against all cancer cells. Interestingly, most of the synthesized derivatives demonstrated IC_{50} values lower than cabozantinib, a reference

kinase inhibitor. Also, the antiproliferative activity of all synthesized compounds was evaluated against NIH3T3 non-cancer cell line. We found that the compounds relatively spare the non-cancer cells compared to malignant cells.

In an attempt to explore the protein kinase inhibitory potential of the most promising compounds, derivatives **4a**, **4b**, **4e**, **4g**, and **4i** were assessed against a panel of major kinases at 10 μ M concentration by a radiometric assay. Benzyl and *p*-methyl benzyl substituted compounds, **4a** and **4i**, showed encouraging inhibitory potentials against CDK2, FLT4 and PDGFRA. This shows that only small lipophilic moieties with optimized bulkiness such as methyl at para position of benzyl pendant could be tolerated to achieve compounds with multi-kinase and CDK2 inhibitory potential. Considering the obtained IC_{50} values of **4a** and **4i** against these three kinases, it is evident that unsubstituted benzyl moiety (**4a**) would be considered as a reasonable pendant for specific targeting of CDK2 and FLT4, while the introduction of methyl group (**4i**) would significantly increase the PDGFRA inhibitory activity.

The anticancer effect of CDK2 inhibition has been observed across a range of cancer types, notably in breast^{23,45}, lung^{46,47}, colon⁴⁸, and PDAC⁴⁹. On the other hand, FLT4 is predominantly expressed on vascular endothelial cells, especially those forming angiogenic vessel sprouts in malignant tumors⁵⁰. FLT4 inhibitors can hinder lymphangiogenesis and suppress tumor metastasis⁵¹. Similarly, PDGFRA aberrant activation is associated with various malignant features, including cell proliferation, metastasis, invasion and angiogenesis⁵², and PDGFRA inhibitors show potential in suppressing multiple tumors⁵³.

Our results indicate that the synthesized compounds show promise as multikinase inhibitors. While multikinase inhibitors offer advantages such as enhanced efficacy and reduced risk of resistance by targeting multiple pathways at the same time and hence hindering the escape mechanisms. Indeed, many of the FDA approved kinase inhibitors fit into the category of multi-targeted agents; For instance, cabozantinib and crizotinib both effectively target several kinases⁵⁴. However, it must also be mentioned that hitting several targets at the same time may also pose challenges, including higher toxicity⁵⁵.

Using RNase/PI flow cytometric assay, compounds **4a**, **4e**, and **4i** were examined for their influence on the population distribution of cancerous cells across various phases of the cell cycle. The results indicated that all three compounds dose-dependently increased the number of cells in the S phase and simultaneously reduced the cells in G2/M phase. These findings are compatible with the CDK2 inhibitory potential of the target compounds, because CDK2 is very well known to have an important roles in the regulation of cell cycle progression^{56,57} and in particular, the progression through the S phase⁵⁸. It has been reported that CDK2/cyclin A inhibitors cause cells to stop in the S or G2/M phases of the cell cycle⁵⁹. Compound **4e** notably increases the sub-G1 phase, indicating a direct cytotoxic effect on the cells. We must emphasize that some of the synthesized compounds may have several additional mechanisms of action and their anticancer effect may not be limited only to kinase inhibitory properties.

Further investigation was conducted on compounds **4a**, **4e**, and **4i** to evaluate their apoptosis induction potential in cancer cells using the Hoechst 33,258 assay that reveals the morphological characteristics of apoptosis. The results revealed evident indications of apoptotic characteristics, such as fragmentation and nuclear shrinkage.

Additionally, computational analyses corroborated our experimental findings and predicted the binding modes of synthetic compounds in CDK2, FLT4, and PDGFRA target active sites. Compound **4a** showed two important hydrogen bond interactions with Asp86 and Leu83, a π - π stacked interaction through Phe82, and several van der Waals interactions to fit on the hydrophobic pocket of the CDK2 kinase domain (Fig. 9B).

Also, compound **4a** was docked into the active site of both FLT4 and PDGFRA targets. According to the Fig. 9D, compound **4a** exhibited hydrogen bond interaction with the key residue of the PDGFRA including Cys677, and Asp836 which are also present in the native ligand imatinib (Fig. 9C). The interaction of compound **4a** with the FLT4 target was also investigated, revealing four hydrogen bond interactions with residues Cys1054, Asn934, Arg1041, and Ser1275, as well as π - σ interactions with Leu1044, Leu1058, and Ala855.

The MD simulation was performed to assess the binding interactions of compound **4a** within the active site of the three targets. The plots of the total number of hydrogen bonds, RMSF, and RMSD indicated that three complexes remained stable throughout the simulation period. The cluster analysis of CDK2-compound **4a** complex revealed two hydrogen bond interaction with Gly12 and Asp85, π - π T-shaped interaction with Phe79, and π -anion interaction with Asp144 (Fig. 11A). The cluster analysis of FLT4-compound **4a** complex predicted three distinct types of interactions: hydrogen bonds formed between Lys879 and Arg1041, a π -sigma interaction involving Val859, and a π -cation interaction with Arg940 residue (Fig. 11B). The cluster analysis of PDGFRA-compound **4a** complex suggested two critical hydrogen bonds with Cys677 and Asp836, an amide- π stacked interaction with Cys835, π - π T-shaped interaction with Phe837, along with a broad hydrophobic interaction with the PDGFRA target (Fig. 11C). In general, compound **4a** forms a strong interaction with the binding pockets of three enzymes, consistent with docking studies.

Finally, the physicochemical properties of novel compounds are demonstrated in Table 5. The finding proved that each new structure complied with Lipinski's rule of five: (HBD \leq 5, HBA \leq 10, lipophilicity (CLog p) \leq 5, and molecular weight \leq 500) although some compounds exceeded the recommended molecular weight. Compounds that violate more than one of Lipinski's rules may encounter challenges related to bioavailability.

A limitation of our work is the lack of knowledge regarding the toxicological profile and pharmacokinetics of synthetic compounds. Therefore, future in vivo studies are necessary to address this important aspect. Moreover, blocking additional cancer targets including kinases as well as other potential molecular targets is also a possibility that cannot be ruled out in the present work and would require additional studies in the future.

Conclusions.

We designed and synthesized 10 novel 1,4-naphthoquinone-1,2,3-triazole hybrid derivatives incorporating various benzyl moieties and phthalimide ring as anticancer agents with multi-kinase inhibitory potential.

The compounds showed high antiproliferative capacity against lung, pancreatic and colorectal cancer cell lines (lowest IC_{50} value: 0.3 μ M) while it relatively spared NIH3T3, the non-cancer cell line. Evaluation of the kinase inhibitory potential of the most promising anticancer agents revealed that compounds **4a** and **4i**, bearing benzyl and *p*-methyl benzyl rings, respectively, inhibit CDK2, FLT4 (VEGFR3), and PDGFRA kinases (lowest IC_{50} value: 0.220 μ M). Induction of apoptosis and S phase arrest were also caused in cancer cells by these compounds. The possible interactions of potent compounds with CDK2, FLT4 and PDGFRA receptors were evaluated by docking study. Furthermore, MD simulation studies of compound **4a** with CDK2, FLT4 (VEGFR3), and PDGFRA enzymes suggested important structural features for biological activity. Finally, the synthesized compounds were investigated through in silico study, and the results complied with Lipinski's rule. The results of this study suggest that 1,4-naphthoquinone derivatives present promising anticancer agents with considerable multi-kinase inhibitory capacity.

Materials and methods

Chemistry

All chemicals and materials were procured from Merck, Fluka, and Sigma-Aldrich commercial providers and were used without additional purification. Thermo Scientific Electrothermal digital equipment (Thermo Fisher Scientific Inc.) was used to determine the melting points of the final compounds using open capillary tubes. Thin layer chromatography (TLC) on aluminum plates coated with silica gel 60 GF254 was performed, with spots detected under UV light (254 nm). The IR spectra of synthetic compounds were acquired by a Perkin-Elmer Spectrum RXI FTIR spectrophotometer, employing KBr disks as the sample medium. 1H NMR (400 MHz and 300 MHz) and ^{13}C NMR (75 MHz) spectra were recorded on a Bruker Avance DPX250 spectrometer at constant temperature and the signals of the NMR spectrums are represented as δ value (ppm) relative to TMS in the downfield direction. Each of the compound's coupling constants (*J*) are stated in hertz (Hz). Spectra characterization was performed utilizing MestReC 14.0.0–23239 (Mestrelab Research S.L, MestReNova) software. Mass spectra were analyzed utilizing Agilent Technology (HP) 7000 triple quadrupole mass spectrometer under an electron impact mode, employing an ionization voltage of 70 electron voltage (eV). CHNS elemental analysis was performed by FLASH EA 1112 SERIES thermo Finnigan equipment.

Synthesis of 1-Nitro-4-(prop-2-yn-1-yloxy)benzene compound (1)

4-Nitro phenol (1 mmol, 1 meq, 0.139 g) and potassium carbonate (3 mmol, 3 meq, 0.41 g) were added to a round bottle flask in 5 mL acetone as the solvent. The suspension was heated for 30 min, followed by the dropwise addition of propargyl bromide (1.2 mmol, 1.2 meq, 0.1 mL). The mixture was refluxed for 5 h. The reaction's progress was tracked using thin-layer chromatography (TLC) until completion. Once cooled, the solid was filtered, rinsed with water, and then subjected to recrystallization from ethanol to yield pure compound **1**.

1-Nitro-4-(prop-2-yn-1-yloxy)benzene (1)⁶⁰. Light yellow solid, mp: 101–103 °C, Yield: 95%; FT-IR (KBr) ν_{max} (cm^{-1}): 3253, 2119, 1595, 1498, 1331, 1249, 1015. 1H NMR (400 MHz, DMSO- d_6) δ_H (ppm): 3.69 (t, H, $J=4$ Hz, $C\equiv CH$), 4.98 (d, 2 H, $J=4$ Hz, $CH_2-C\equiv C$), 7.16–7.22 (m, 2 H, Ar-H), 8.18–8.26 (m, 2 H, Ar-H). ^{13}C NMR (100 MHz, DMSO- d_6) δ_C (ppm): 56.7, 78.6, 79.6, 115.9 (2 C), 126.2 (2 C), 141.8, 162.8.

Synthesis of substituted derivatives of 1-Benzyl-4-((4-nitrophenoxy)methyl)-1H-1,2,3-triazole (2a-j)

Various derivatives of (**2a-j**) were synthesized by reacting the appropriate aryl halide (1.1 mmol, 1.1 meq) with sodium azide (1 mmol, 1 meq, 0.065 g) in triethylamine (TEA) as a base, using t-BuOH/water as the solvent. Following approximately 30 min, 1-nitro-4-(prop-2-yn-1-yloxy) benzene compound (**1**) (1 mmol, 1 meq, 0.17 g) dissolved in absolute t-BuOH (5 ml) was added to the mixture alongside with $CuSO_4 \cdot 5H_2O$ (0.075 mmol, 0.075 meq, 0.015 g, 10 mol%) and Sodium ascorbate (0.75 mmol, 0.75 meq, 0.148 g, 25 mol%). The reaction was conducted at 40 °C and mixed continuously for 48 h. Following confirming the reaction's completion, verified by TLC analysis, the solvent was removed under vacuum, washed with water and the resulting residue was purified by recrystallization from a mixture of ethyl acetate and n-hexane to isolate the desired compound ⁶¹.

Synthesis of 1-Benzyl-4-((4-nitrophenoxy)methyl)-1H-1,2,3-triazole (2a): Yellow solid, mp: 94–96 °C, Yield: 92%; FT-IR (KBr) ν_{max} (cm^{-1}): 1595, 1496, 1337, 1265, 1113. 1H NMR (300 MHz, DMSO- d_6) δ_H (ppm): 5.32 (s, 2 H, N- CH_2 -Ph), 5.62 (s, 2 H, CH_2-O -Ph), 7.20–7.33 (m, 4 H, Ar-H), 7.54–7.64 (m, 2 H, Ar-H), 8.17–8.28 (m, 2 H, Ar-H), 8.36 (s, H, triazole-H). ^{13}C NMR (100 MHz, DMSO- d_6) δ_C (ppm): 53.3, 62.3, 115.8 (2 C), 125.5, 126.3 (2 C), 128.4 (2 C), 128.6, 129.2 (2 C), 136.4, 141.5, 142.5, 163.7.

Synthesis of substituted derivatives 4-((1-Benzyl-1H-1,2,3-triazol-4-yl)methoxy)aniline (3a-3j)

Compound **2a-2j** (1.1 mmol, 1.1 meq) dissolved in EtOH/ H_2O (8:2) as a solvent at 60 °C and hydrazine hydrate (0.25 mmol, 0.12 meq, 0.08 mL) was added. Subsequently, a small quantity of Raney Ni (0.25 mL) was added. After allowing the solution to proceed (15 to 60 min), the hot solution was filtered to remove the Ni and the solvent was then evaporated to gain a light-yellow solid. This solid was washed with water and recrystallization in EtOH and H_2O (8:2) ⁶².

4-((1-Benzyl-1H-1,2,3-triazol-4-yl)methoxy)aniline (3a): Yellow solid, mp: 106–108 °C, Yield: 92%; FT-IR (KBr) ν_{max} (cm^{-1}): 3370, 3308, 1598, 1506, 1236, 1045. 1H NMR (300 MHz, DMSO- d_6) δ_H (ppm): 4.71 (s, 2 H, NH_2), 5.01 (s, 2 H, CH_2-O -Ph), 5.63 (s, 2 H, N- CH_2 -Ph), 6.46–6.59 (m, 2 H, Ar-H), 6.76 (d, $J=9$ Hz, 2 H, Ar-H), 7.3 (d, $J=6$ Hz, 2 H, Ar-H), 7.62 (d, $J=9$ Hz, 2 H, Ar-H), 8.27 (s, H, triazole-H). ^{13}C NMR (100 MHz, DMSO- d_6) δ_C (ppm): 53.2, 62.2, 115.3 (2 C), 116.2 (2 C), 124.9, 128.3 (2 C), 128.6, 129.2 (2 C), 136.5, 143.2, 144.1, 149.8.

4-((1-(4-Bromobenzyl)-1H-1,2,3-triazol-4-yl)methoxy)aniline (3b): Light pink solid, mp: 112–114 °C, Yield: 86%; FT-IR (KBr) ν_{max} (cm^{-1}): 3458, 3369, 1607, 1507, 1225, 1006. 1H NMR (400 MHz, DMSO- d_6) δ_H (ppm): 4.66 (s, 2 H, NH_2), 4.97 (s, 2 H, CH_2-O -Ph), 5.60 (s, 2 H, N- CH_2 -Ph), 6.48–6.53 (m, 2 H, Ar-H),

6.69–6.74 (m, 2 H, Ar–H), 7.24–7.31 (m, 2 H, Ar–H), 7.56–7.61 (m, 2 H, Ar–H), 8.22 (s, H, triazole-H). ^{13}C NMR (100 MHz, DMSO- d_6) δ_{C} (ppm): 52.5, 62.2, 115.3 (2 C), 116.2 (2 C), 121.8, 124.9, 130.6 (2 C), 132.1 (2 C), 135.9, 143.2, 144.1, 149.8.

4-((1-(4-Fluorobenzyl)-1H-1,2,3-triazol-4-yl)methoxy)aniline (3c): Cream solid, mp: 98–100 °C, Yield: 91%; FT-IR (KBr) ν_{max} (cm^{-1}): 3451, 3337, 1618, 1507, 1224, 1006. ^1H NMR (400 MHz, DMSO- d_6) δ_{H} (ppm): 4.66 (s, 2 H, NH_2), 4.97 (s, 2 H, CH_2 –O–Ph), 5.60 (s, 2 H, N– CH_2 –Ph), 6.48–6.53 (m, 2 H, Ar–H), 6.69–6.75 (m, 2 H, Ar–H), 7.18–7.25 (m, 2 H, Ar–H), 7.35–7.41 (m, 2 H, Ar–H), 8.22 (s, H, triazole-H). ^{13}C NMR (100 MHz, DMSO- d_6) δ_{C} (ppm): 52.4, 62.2, 115.3 (2 C), 115.9, 116.2 (2 C), 124.8, 126.3, 130.7, 132.8, 132.8, 143.2, 144.1, 149.7, 161.1.

4-((1-(4-Chlorobenzyl)-1H-1,2,3-triazol-4-yl)methoxy)aniline (3d): Caramel solid, mp: 110–112 °C, Yield: 88%; FT-IR (KBr) ν_{max} (cm^{-1}): 3458, 3368, 1621, 1507, 1226, 1007. ^1H NMR (400 MHz, DMSO- d_6) δ_{H} (ppm): 4.68 (s, 2 H, NH_2), 4.97 (s, 2 H, CH_2 –O–Ph), 5.61 (s, 2 H, N– CH_2 –Ph), 6.47–6.54 (m, 2 H, Ar–H), 6.69–6.75 (m, 2 H, Ar–H), 7.29–7.37 (m, 2 H, Ar–H), 7.41–7.47 (m, 2 H, Ar–H), 8.22 (s, H, triazole-H). ^{13}C NMR (100 MHz, DMSO- d_6) δ_{C} (ppm): 52.4, 62.2, 115.3 (2 C), 116.2 (2 C), 124.9, 129.2 (2 C), 130.3 (2 C), 133.3, 135.5, 143.2, 144.1, 149.8.

4-((1-(3,4-Dichlorobenzyl)-1H-1,2,3-triazol-4-yl)methoxy)aniline (3e): Yellow solid, mp: 116–118 °C, Yield: 84%; FT-IR (KBr) ν_{max} (cm^{-1}): 3450, 3397, 1626, 1508, 1226, 1019. ^1H NMR (400 MHz, DMSO- d_6) δ_{H} (ppm): 4.66 (s, 2 H, NH_2), 4.98 (s, 2 H, CH_2 –O–Ph), 5.63 (s, 2 H, N– CH_2 –Ph), 6.48–6.53 (m, 2 H, Ar–H), 6.69–6.74 (m, 2 H, Ar–H), 7.24–7.31 (m, H, Ar–H), 7.61–7.67 (m, 2 H, Ar–H), 8.27 (s, H, triazole-H). ^{13}C NMR (100 MHz, DMSO- d_6) δ_{C} (ppm): 51.8, 62.2, 115.3 (2 C), 116.2 (2 C), 125.0, 126.3, 128.8, 130.5, 131.5, 131.7, 137.5, 143.3, 144.2, 149.7.

4-((1-(3-Chlorobenzyl)-1H-1,2,3-triazol-4-yl)methoxy)aniline (3f): light chocolate solid, mp: 85–87 °C, Yield: 87%; FT-IR (KBr) ν_{max} (cm^{-1}): 3385, 3315, 1637, 1508, 1227, 1050. ^1H NMR (400 MHz, DMSO- d_6) δ_{H} (ppm): 4.67 (s, 2 H, NH_2), 4.98 (s, 2 H, CH_2 –O–Ph), 5.63 (s, 2 H, N– CH_2 –Ph), 6.48–6.53 (m, 2 H, Ar–H), 6.68–6.76 (m, 2 H, Ar–H), 7.22–7.29 (m, H, Ar–H), 7.38–7.43 (m, 3 H, Ar–H), 8.26 (s, H, triazole-H). ^{13}C NMR (100 MHz, DMSO- d_6) δ_{C} (ppm): 52.4, 62.2, 115.3 (2 C), 116.2 (2 C), 125.0, 127.1, 128.2, 128.6, 131.2, 133.7, 138.9, 143.2, 144.2, 149.8.

4-((1-(4-Isopropylbenzyl)-1H-1,2,3-triazol-4-yl)methoxy)aniline (3 g): Cream solid, mp: 102–104 °C, Yield: 88%; FT-IR (KBr) ν_{max} (cm^{-1}): 3383, 3321, 1643, 1510, 1235, 1050. ^1H NMR (400 MHz, DMSO- d_6) δ_{H} (ppm): 1.18 (d, 6 H, $J=8$ Hz, CH_3 (Isopropyl)), 2.79–2.92 (m, 1H, CH_2 (Isopropyl)), 4.67 (s, 2 H, NH_2), 4.96 (s, 2 H, CH_2 –O–Ph), 5.55 (s, 2 H, N– CH_2 –Ph), 6.45–6.53 (m, 2 H, Ar–H), 6.69–6.74 (m, 2 H, Ar–H), 7.22–7.28 (m, 4 H, Ar–H), 8.20 (s, H, triazole-H). ^{13}C NMR (100 MHz, DMSO- d_6) δ_{C} (ppm): 24.2 (2 C, CH_3), 33.6 (CH), 53.0, 62.2, 115.3 (2 C), 116.2 (2 C), 124.7, 127.1 (2 C), 128.5 (2 C), 133.9, 143.1, 144.0, 148.8, 149.8.

4-((1-(4-tert-Butylbenzyl)-1H-1,2,3-triazol-4-yl)methoxy)aniline (3 h): Light yellow solid, mp: 93–95 °C, Yield: 89%; FT-IR (KBr) ν_{max} (cm^{-1}): 3386, 3321, 1640, 1509, 1235, 1050. ^1H NMR (400 MHz, DMSO- d_6) δ_{H} (ppm): 1.26 (s, 9 H, –C (CH_3) $_3$), 4.66 (s, 2 H, NH_2), 4.96 (s, 2 H, CH_2 –O–Ph), 5.55 (s, 2 H, N– CH_2 –Ph), 6.48–6.54 (m, 2 H, Ar–H), 6.69–6.75 (m, 2 H, Ar–H), 7.22–7.28 (m, 2 H, Ar–H), 7.36–7.42 (m, 2 H, Ar–H), 8.20 (s, H, triazole-H). ^{13}C NMR (100 MHz, DMSO- d_6) δ_{C} (ppm): 31.5 (3 C), 34.7, 52.9, 62.2, 115.3 (2 C), 116.1 (2 C), 124.7, 126.0 (2 C), 128.2 (2 C), 133.6, 143.2, 144.1, 149.8, 151.1.

4-((1-(4-Methylbenzyl)-1H-1,2,3-triazol-4-yl)methoxy)aniline (3i): Cream solid, mp: 98–100 °C, Yield: 83%; FT-IR (KBr) ν_{max} (cm^{-1}): 3429, 3324, 1629, 1508, 1223, 1043. ^1H NMR (400 MHz, DMSO- d_6) δ_{H} (ppm): 2.29 (s, 3 H, (CH_3)), 4.78 (s, 2 H, NH_2), 4.96 (s, 2 H, CH_2 –O–Ph), 5.54 (s, 2 H, N– CH_2 –Ph), 6.48–6.56 (m, 2 H, Ar–H), 6.69–6.76 (m, 2 H, Ar–H), 7.15–7.24 (m, 4 H, Ar–H), 8.17 (s, H, triazole-H). ^{13}C NMR (100 MHz, DMSO- d_6) δ_{C} (ppm): 21.1, 53.0, 62.2, 115.4 (2 C), 116.2 (2 C), 124.7, 128.4 (2 C), 129.7 (2 C), 133.5, 137.9, 142.8, 144.7, 149.9.

2-((4-((4-Aminophenoxy)methyl)-1H-1,2,3-triazol-1-yl)methyl)phenethyl isoindoline-1,3-dione (3j): Brown solid, mp: 120–122 °C, Yield: 53%; FT-IR (KBr) ν_{max} (cm^{-1}): 3234, 3205, 1586, 1505, 1249, 1051. ^1H NMR (400 MHz, DMSO- d_6) δ_{H} (ppm): 3.99–4.05 (m, 2 H, CO–N– CH_2 – CH_2), 4.64–4.70 (m, 2 H, N=N–N– CH_2 – CH_2), 4.99 (s, 2 H, NH_2), 5.29 (s, 2 H, CH_2 –O–Ph), 5.39 (s, 2 H, N– CH_2 –Ph), 7.19–7.31 (m, 8 H, Ar–H), 7.83 (s, H, triazole-H), 8.21–8.26 (m, 4 H, Ar–H). ^{13}C NMR (100 MHz, DMSO- d_6) δ_{C} (ppm): 56.7, 62.1, 67.1, 79.6, 109.6, 115.8 (2 C), 115.9, 123.6, 125.8, 126.2 (2 C), 126.3, 131.8, 134.9, 137.7, 141.4, 141.6, 141.8, 142.2, 142.9, 162.8, 163.2, 163.6, 167.8 (2 C).

Synthesis of substituted derivatives 2-((4-((1-Benzyl-1H-1,2,3-triazol-4-yl)methoxy) phenyl) amino)naphthalene-1,4-dione (4a–4j)

Several derivatives of **4a–4j** were produced by reacting 1,4-Naphthoquinones (1.2 mmol, 1.2 meq, 0.18 g) with **3a–3j** derivatives in EtOH at room temperature. The reaction progressed until the color changed (1 to 4 h) evident by TLC analysis in EtOAc/ n-hexane (4:6), resulting in the formation of the final compound, which was then subjected to recrystallization in EtOH.

2-((4-((1-Benzyl-1H-1,2,3-triazol-4-yl)methoxy)phenyl)amino)naphthalene-1,4-dione (4a). Red solid, mp: 177–179 °C, Yield: 93%; FT-IR (KBr) ν_{max} (cm^{-1}): 3310, 1671, 1623, 1600, 1571, 1507, 1353, 1306, 1241. ^1H NMR (300 MHz, DMSO- d_6) δ_{H} (ppm): 5.17 (s, 2 H, CH_2 –O–Ph), 5.63 (s, 2 H, N– CH_2 –Ph), 5.94 (s, 1H, 1,4-Naphthoquinone (1,4-NQ)-H), 7.11 (d, $J=9$ Hz, 2 H, Ar–H), 7.28–7.38 (m, 7 H, Ar–H), 7.77 (t, $J=6$ Hz, 1H, 1,4-NQ-H), 7.85 (t, $J=6$ Hz, 1H, 1,4-NQ-H), 7.94 (d, $J=6$ Hz, 1H, 1,4-NQ-H), 8.05 (d, $J=6$ Hz, 1H, 1,4-NQ-H), 8.33 (s, 1H, Triazole-H), 9.20 (s, 1H, NH). ^{13}C NMR (75 MHz, DMSO- d_6) δ_{C} (ppm): 53.3, 61.7, 101.6, 115.8 (2 C), 125.2, 125.7, 126.0 (2 C), 126.5, 128.4 (2 C), 128.7, 129.3 (2 C), 130.9, 131.4, 133.0, 133.2, 135.4, 136.5, 143.4, 147.3, 156.1, 182.1 (C=O), 182.7 (C=O). MS (EI) m/z (%): 438 ($[\text{M}+2]$, 4), 436 (M^+ , 70), 265 (100), 173 (26), 91 (78), 144 (42). Anal. Calcd for $\text{C}_{26}\text{H}_{20}\text{N}_4\text{O}_3$: C 71.55; H 4.62; N 12.84%; found: C 70.49, H 4.58, N 13.24%.

2-((4-((1-(4-Bromobenzyl)-1H-1,2,3-triazol-4-yl)methoxy)phenyl)amino) naphthalene-1,4-dione (4b). Violet solid, mp: 172–174 °C, Yield: 96%; FT-IR (KBr) ν_{\max} (cm⁻¹): 3231, 1675, 1596, 1568, 1507, 1355, 1292, 1241. ¹H NMR (300 MHz, CDCl₃) δ_{H} (ppm): 5.22 (s, 2 H, CH₂-O-Ph), 5.53 (s, 2 H, N-CH₂-Ph), 6.23 (s, 1H, 1,4-NQ-H), 7.02 (d, *J* = 9 Hz, 2 H, Ar-H), 7.19–7.23 (m, 4 H, Ar-H), 7.46 (s, 1H, NH), 7.53 (d, *J* = 9 Hz, 2 H, Ar-H), 7.58 (s, 1H, Triazole-H), 7.68 (t, *J* = 9 Hz, 1H, 1,4-NQ-H), 7.77 (t, *J* = 9 Hz, 1H, 1,4-NQ-H), 8.08–8.15 (m, 2 H, 1,4-NQ-H). ¹³C NMR (75 MHz, CDCl₃) δ_{C} (ppm): 53.6, 62.3, 102.6, 115.8 (2 C), 122.7, 123.1, 124.9 (2 C), 126.2, 126.5, 129.8 (2 C), 130.4, 130.6, 132.3, 132.4 (2 C), 133.3, 133.4, 134.9, 144.5, 145.6, 156.1, 182.1, 183.8. MS (EI) *m/z* (%): 517 ([*M* + 2], 15), 515 (*M*⁺, 15), 265 (100), 264 (66), 169 (42), 171 (41), 90 (14). Anal. Calcd for C₂₆H₁₉BrN₄O₃: C 60.59; H 3.72; N 10.87%; found: C 59.95, H 3.69, N 11.20%.

2-((4-((1-(4-Fluorobenzyl)-1H-1,2,3-triazol-4-yl)methoxy)phenyl)amino) naphthalene-1,4-dione (4c). Dark violet solid, mp: 190–192 °C, Yield: 94%; FT-IR (KBr) ν_{\max} (cm⁻¹): 3307, 1667, 1601, 1570, 1510, 1354, 1298, 1221. ¹H NMR (300 MHz, DMSO-*d*₆) δ_{H} (ppm): 5.17 (s, 2 H, CH₂-O-Ph), 5.63 (s, 2 H, N-CH₂-Ph), 5.95 (s, 1H, 1,4-NQ-H), 7.11 (d, *J* = 9 Hz, 2 H, Ar-H), 7.24 (d, *J* = 9 Hz, 2 H, Ar-H), 7.30 (d, *J* = 9 Hz, 2 H, Ar-H), 7.38–7.48 (m, 2 H, Ar-H), 7.72–7.89 (m, 2 H, 1,4-NQ-H), 8.90–8.98 (m, 1H, 1,4-NQ-H), 8.04 (d, *J* = 9 Hz, 1H, 1,4-NQ-H), 8.33 (s, 1H, Triazole-H), 9.20 (s, 1H, NH). ¹³C NMR (75 MHz, DMSO-*d*₆) δ_{C} (ppm): 52.5, 61.7, 101.6, 115.8 (2 C), 116.0, 116, 3, 125.2, 125.7, 126.0 (2 C), 126.5, 130.8, 130.9 (2 C), 131.4, 132.8, 132.8, 133.0, 133.2, 135.4, 143.4, 147.3, 156.1, 182.1 (C=O), 182.8 (C=O). MS (EI) *m/z* (%): 456 ([*M* + 2], 2), 454 (*M*⁺, 34), 265 (98), 264 (70), 191 (26), 162 (30), 109 (100). Anal. Calcd for C₂₆H₁₉FN₄O₃: C 68.72; H 4.21; N 12.33%; found: C 68.20, H 4.30, N 12.79%.

2-((4-((1-(4-Chlorobenzyl)-1H-1,2,3-triazol-4-yl)methoxy)phenyl)amino) naphthalene-1,4-dione (4d). Purple solid, mp: 164–166 °C, Yield: 92%; FT-IR (KBr) ν_{\max} (cm⁻¹): 3234, 1672, 1616, 1598, 1589, 1508, 1351, 1291, 1238, 1216. ¹H NMR (300 MHz, CDCl₃) δ_{H} (ppm): 5.22 (s, 2 H, CH₂-O-Ph), 5.54 (s, 2 H, N-CH₂-Ph), 6.23 (s, 1H, 1,4-NQ-H), 7.02 (d, *J* = 9 Hz, 2 H, Ar-H), 7.18–7.26 (m, 4 H, Ar-H), 7.38 (d, 2 H, *J* = 6 Hz, Ar-H), 7.46 (s, 1H, NH), 7.58 (s, 1H, Triazole-H), 7.67 (t, *J* = 6 Hz, 1H, 1,4-NQ-H), 7.77 (t, *J* = 6 Hz, 1H, 1,4-NQ-H), 8.08–8.15 (m, 2 H, 1,4-NQ-H). ¹³C NMR (75 MHz, CDCl₃) δ_{C} (ppm): 53.6, 62.3, 102.6, 115.8 (2 C), 122.7, 124.9 (2 C), 126.2, 126.5, 129.4 (2 C), 129.5 (2 C), 130.4, 130.6, 132.3, 132.9, 133.3, 135.0 (2 C), 144.5, 145.6, 156.1, 182.1, 183.8. MS (EI) *m/z* (%): 472 ([*M* + 2], 14), 470 (*M*⁺, 44), 265 (100), 264 (71), 207 (17), 125 (59). Anal. Calcd for C₂₆H₁₉ClN₄O₃: C 66.32; H 4.07; N 11.90%; found: C 66.19, H 3.94, N 11.18%.

2-((4-((1-(3,4-Dichlorobenzyl)-1H-1,2,3-triazol-4-yl)methoxy)phenyl)amino) naphthalene-1,4-dione (4e). Violet solid, mp: 179–181 °C, Yield: 82%; FT-IR (KBr) ν_{\max} (cm⁻¹): 3444, 1678, 1623, 1596, 1575, 1520, 1353, 1247. ¹H NMR (300 MHz, CDCl₃) δ_{H} (ppm): 5.23 (s, 2 H, CH₂-O-Ph), 5.52 (s, 2 H, N-CH₂-Ph), 6.22 (s, 1H, 1,4-NQ-H), 6.96–7.07 (m, 2 H, Ar-H), 7.09–7.25 (m, 3 H, Ar-H), 7.34–7.52 (m, 2 H, Ar-H & s, 1H, NH), 7.59–7.72 (m, 2 H, 1,4-NQ-H), 7.76 (s, 1H, Triazole-H), 8.04–8.17 (m, 2 H, 1,4-NQ-H). ¹³C NMR (75 MHz, CDCl₃) δ_{C} (ppm): 53.0, 62.3, 102.6, 115.8 (2 C), 122.7, 124.9 (2 C), 126.2, 126.5, 127.3, 129.3, 123.0 (2 C), 130.4, 130.7, 131.2, 132.3, 133.3, 134.6, 134.9, 144.7, 145.6, 156.1, 182.1, 183.8. MS (EI) *m/z* (%): 506 ([*M* + 2], 17), 504 (*M*⁺, 25), 265 (100), 264 (74), 159 (45). Anal. Calcd for C₂₆H₁₈Cl₂N₄O₃: C 61.80; H 3.59; N 11.09%; found: C 61.84, H 3.59, N 11.05%.

2-((4-((1-(3-Chlorobenzyl)-1H-1,2,3-triazol-4-yl)methoxy)phenyl)amino) naphthalene-1,4-dione (4f). Light violet solid, mp: 168–170 °C, Yield: 87%; FT-IR (KBr) ν_{\max} (cm⁻¹): 3244, 1674, 1613, 1601, 1572, 1353, 1295. ¹H NMR (300 MHz, CDCl₃) δ_{H} (ppm): 5.23 (s, 2 H, CH₂-O-Ph), 5.55 (s, 2 H, N-CH₂-Ph), 6.23 (s, 1H, 1,4-NQ-H), 7.02 (d, *J* = 9 Hz, 2 H, Ar-H), 7.14–7.23 (m, 4 H, Ar-H), 7.32–7.37 (m, 2 H, Ar-H), 7.47 (s, 1H, NH), 7.62 (s, 1H, Triazole-H), 7.66 (t, *J* = 9 Hz, 1,4-NQ-H), 7.76 (t, *J* = 9 Hz, 1H, 1,4-NQ-H), 8.06–8.14 (m, 2 H, 1,4-NQ-H). ¹³C NMR (75 MHz, CDCl₃) δ_{C} (ppm): 53.6, 62.3, 102.6, 115.8 (2 C), 122.8, 124.9 (2 C), 126.1, 126.2, 126.5, 128.2, 129.1, 130.4, 130.5, 130.6, 132.9, 133.3, 135.0, 135.1, 136.4, 144.5, 145.6, 156.1, 182.1, 183.8. MS (EI) *m/z* (%): 472 ([*M* + 2], 10), 470 (*M*⁺, 26), 265 (100), 264 (67), 207 (22), 125 (54). Anal. Calcd for C₂₆H₁₉ClN₄O₃: C 66.32; H 4.07; N 11.90%; found: C 66.32, H 3.97, N 11.92%.

2-((4-((1-(4-Isopropylbenzyl)-1H-1,2,3-triazol-4-yl)methoxy)phenyl)amino) naphthalene-1,4-dione (4g). Dark red solid, mp: 182–185 °C, Yield: 78%; FT-IR (KBr) ν_{\max} (cm⁻¹): 3343, 1667, 1616, 1605, 1520, 1303, 1244. ¹H NMR (300 MHz, CDCl₃) δ_{H} (ppm): 1.25 (d, 6 H, *J* = 9 Hz, CH₃ (Isopropyl)), 2.87–2.97 (m, 1H, CH₂ (Isopropyl)), 5.20 (s, 2 H, CH₂-O-Ph), 5.53 (s, 2 H, N-CH₂-Ph), 6.23 (s, 1H, 1,4-NQ-H), 7.02 (d, *J* = 9 Hz, 2 H, Ar-H), 7.17–7.26 (m, 6 H, Ar-H), 7.48 (s, 1H, NH), 7.58 (s, 1H, Triazole-H), 7.66 (t, *J* = 9 Hz, 1H, 1,4-NQ-H), 7.76 (t, *J* = 9 Hz, 1H, 1,4-NQ-H), 8.07–8.13 (m, 2 H, 1,4-NQ-H). ¹³C NMR (75 MHz, CDCl₃) δ_{C} (ppm): 23.9 (2 C, CH₃), 33.9 (CH), 54.1, 62.3, 102.6, 115.8 (2 C), 122.7, 124.8 (2 C), 126.2, 126.5, 127.3 (2 C), 128.3 (2 C), 130.4, 130.5, 131.7, 132.3, 133.3, 134.9, 144.1, 145.6, 149.8, 156.2, 182.1, 183.8. MS (EI) *m/z* (%): 480 ([*M* + 2], 2), 478 (*M*⁺, 36), 265 (76), 264 (41), 236 (10), 215 (23), 133 (100). Anal. Calcd for C₂₉H₂₆N₄O₃: C 72.79; H 5.48; N 11.71%; found: C 72.83, H 5.20, N 10.72%.

2-((4-((1-(4-Tert-butylbenzyl)-1H-1,2,3-triazol-4-yl)methoxy)phenyl)amino) naphthalene-1,4-dione (4h). Red solid, mp: 212–215 °C, Yield: 76%; FT-IR (KBr) ν_{\max} (cm⁻¹): 3445, 1626, 1608, 1458, 1248. ¹H NMR (300 MHz, CDCl₃) δ_{H} (ppm): 1.33 (s, 9 H, -C(CH₃)₃), 5.20 (s, 2 H, CH₂-O-Ph), 5.54 (s, 2 H, N-CH₂-Ph), 6.24 (s, 1H, 1,4-NQ-H), 7.02 (d, *J* = 9 Hz, 2 H, Ar-H), 7.22 (dd, *J* = 9 Hz, 4 H, Ar-H), 7.42 (d, *J* = 6 Hz, 2 H, Ar-H), 7.47 (s, 1H, NH), 7.58 (s, 1H, Triazole-H), 7.66 (t, *J* = 6 Hz, 1H, 1,4-NQ-H), 7.76 (t, *J* = 6 Hz, 1H, 1,4-NQ-H), 8.07–8.14 (m, 2 H, 1,4-NQ-H). ¹³C NMR (75 MHz, CDCl₃) δ_{C} (ppm): 31.3 (3 C), 34.7, 54.0, 62.4, 102.6, 115.8 (2 C), 122.7, 124.8 (2 C), 126.1 (2 C), 126.5, 128.0 (2 C), 130.4, 130.6, 131.4, 132.3, 133.4, 134.9, 144.1, 145.6, 152.0, 156.2, 182.1, 183.8. MS (EI) *m/z* (%): 494 ([*M* + 2], 5), 492 (*M*⁺, 66), 265 (89), 264 (49), 229 (24), 147 (100). Anal. Calcd for C₂₉H₂₈N₄O₃: C 73.15; H 5.73; N 11.37%; found: C 73.13, H 5.57, N 11.15%.

2-((4-((1-(4-Methylbenzyl)-1H-1,2,3-triazol-4-yl)methoxy)phenyl)amino) naphthalene-1,4-dione (4i). Red solid, mp: 187–191 °C, Yield: 79%; FT-IR (KBr) ν_{\max} (cm⁻¹): 3293, 1675, 1595, 1584, 1515, 1303, 1241. ¹H NMR (300 MHz, DMSO-*d*₆) δ_{H} (ppm): 2.38 (s, 3 H, (CH₃)), 5.21 (s, 2 H, CH₂-O-Ph), 5.53 (s, 2 H, N-CH₂-Ph), 6.24 (s, 1H, 1,4-NQ-H), 7.03 (d, *J* = 9 Hz, 2 H, Ar-H), 7.17–7.24 (m, 6 H, Ar-H), 7.45 (s, 1H, NH),

7.55 (s, 1H, Triazole-H), 7.64–7.72 (m, 1H, 1,4-NQ-H), 7.78 (t, $J=6$ Hz, 1H, 1,4-NQ-H), 8.09–8.16 (m, 2 H, 1,4-NQ-H). ^{13}C NMR (75 MHz, DMSO- d_6) δ_{C} (ppm): 21.2 (CH_3), 53.1, 61.7, 101.5, 115.8 (2 C), 125.1, 125.7, 126.0 (2 C), 126.5, 128.5 (2 C), 129.8 (2 C), 130.9, 131.4, 133.0, 133.2, 133.5, 135.4, 138.0, 143.3, 147.3, 156.1, 182.1, 182.8. MS (EI) m/z (%): 452 ($[\text{M}+2]$, 2), 450 (M^+ , 40), 265 (61), 264 (37), 236 (9), 187 (20), 158 (37), 105 (100). Anal. Calcd for $\text{C}_{27}\text{H}_{22}\text{N}_4\text{O}_3$: C 71.99; H 4.92; N 12.44%; found: C 70.39, H 4.58, N 10.69%.

2-(2-(4-((1,4-Dioxo-1,4-dihydronaphthalen-2-yl)amino)phenoxy)methyl)-1H-1,2,3-triazol-1-yl)ethyl)isoindoline-1,3-dione (4j). Purple solid, mp: 254–257 °C, Yield: 62%; FT-IR (KBr) ν_{max} (cm^{-1}): 3447, 2960, 2922, 1713, 1678, 1628, 1608, 1493, 1394, 1213. ^1H NMR (300 MHz, DMSO- d_6) δ_{H} (ppm): 3.95–4.06 (m, 2 H, $\text{CO}-\text{N}-\text{CH}_2-\text{CH}_2$), 4.61–4.72 (m, 2 H, $\text{N}=\text{N}-\text{N}-\text{CH}_2-\text{CH}_2$), 5.12 (s, 1H, 1,4-NQ-H), 5.28 (s, 2 H, $\text{CH}_2-\text{O}-\text{Ph}$), 7.17–7.26 (m, 4 H, Ar-H), 7.79–7.87 (m, 4 H, Ar-H), 8.19 (d, $J=9$ Hz, 2 H, 1,4-NQ-H), 8.31–8.36 (m 2 H, 1,4-NQ-H), 8.50 (s, 1H, Triazole-H), 9.20 (s, 1H, NH). ^{13}C NMR (75 MHz, DMSO- d_6) δ_{C} (ppm): 14.0, 19.1, 30.4, 64.5, 115.8, 123.6, 124.5, 125.8, 126.0, 126.3, 129.1 (2 C), 131.5, 131.8, 132.0 (2 C), 132.2, 135.0, 137.6, 139.6, 141.0, 142.2, 152.6, 155.2, 163.7, 167.5, 168.9, 173.5. MS (EI) m/z (%): 521 ($[\text{M}+2]$, 2), 519 (M^+ , 10), 265 (69), 227 (51), 130 (34), 160 (100).

Biological study

Cell culture

Human PDAC cells, Mia-Paca-2, and human lung adenocarcinoma cells, EBC-1, were purchased from the Japanese Collection of Research Bio Resources Cell Bank (JCRB). The pancreatic ductal adenocarcinoma (PDAC) cells, AsPC-1, the colorectal adenocarcinoma cells, HT-29, and breast adenocarcinoma cells, MCF-7, all of human origin were provided from Iranian Biological Resource Center in Tehran, Iran. The cell culture media, including DMEM and RPMI 1640, as well as streptomycin as antibiotics, fetal bovine serum (FBS), and penicillin, were procured from Gibco (Thermo Fisher Scientific). The EBEWE Pharma, Unterach am Attersee, Austria provided cisplatin, doxorubicin, and 3-(4,5-Dimethylthiazol-2-yl)-2,5-diphenyltetrazolium bromide (MTT). Cabozantinib was obtained from LC Laboratories, Woburn, MA, USA. HT-29 cells were maintained in culture media consisting of high-glucose DMEM with 15% FBS, while Mia-Paca-2 cells were grown in a culture media composed of low-glucose DMEM containing 10% FBS. A 10% FBS supplement was included in the RPMI 1640 media for all other cell lines to sustain their optimal growth. Penicillin and streptomycin were added to all growth media. All cell lines were grown in monolayer cultures at a temperature of 37 °C within a humidified incubator, which was set to maintain a controlled atmosphere with 5% CO_2 .

MTT assay

The viability of cancer cells following treatment with synthetic compounds was evaluated using the MTT reduction assay, as reported previously^{63,64}. In brief, the cells were cultured in 96-well plates at various densities for EBC-1 (100×10^3), AsPC-1 (20×10^3), Mia-Paca-2 (7.5×10^3), HT-29 (30×10^3), MCF-7 (30×10^3), NIH3T3 (40×10^3). All compounds, both synthetic and reference, were initially dissolved in dimethyl sulfoxide (DMSO) and then further diluted in the culture medium to a minimum of 400-fold to achieve the desired concentration. After 24 h, duplicate wells were treated with test compounds at different concentrations. Synthetic derivatives were tested at variant concentrations between 0.05 and 100 μM . Reference compounds included doxorubicin, cisplatin and cabozantinib. After an additional incubation of 72 h at 37 °C, the media in each well was replaced with an equal volume of fresh growth media containing 0.5 mg/mL MTT, followed by a 4-hour incubation at 37 °C to allow the formazan crystals to form. In each well, the DMSO was added to dissolve the formazan crystals after a one-hour incubation, followed by a 30-minute shaking period. Ultimately, a microplate reader was used to measure the absorbance of the resulting solutions at 570 nm. The IC_{50} value of each compound was calculated by CurveExpert 1.34 software. Each experiment was repeated a minimum of 3 to 5 times to enhance the credibility and reliability of the results.

Kinase inhibition experiment

In order to assess the kinase inhibitory activity of the most promising compounds as antiproliferative agents including **4a**, **4b**, **4e**, **4g**, and **4i** against crucial oncogenic kinases, a radiometric assay was used. The compounds **4a** and **4e** were tested against a panel of 30 kinases at 10 μM , while the other 3 compounds were examined against some the most important ones.

Furthermore, the activities of compounds **4a** and **4i** against CDK2/cyclin A, VEGFR3, and PDGFR α were evaluated at five concentrations to generate dose-response curves, and IC_{50} values were calculated through curve fitting. These assays were carried out by Eurofins Discovery (Eurofins Cerep, Celle-Lévescault, France).

Cell cycle test

The effect of select compounds (**4a**, **4e**, and **4i**) on the cell cycle distribution of AsPC-1 cells was examined by propidium iodide (PI)-RNase flow cytometric assay to acquire additional insight into the mechanism of action of these derivatives⁶⁵. AsPC-1 cells were seeded in 12-well microplates at a density of 2×10^5 cells/mL (1 mL per well) and incubated overnight. Later, different concentrations of **4a**, **4e**, and **4i** derivatives at 3, 10, 30, and 50 μM were added to different wells. The cells were collected after trypsinization and collected into small tubes during 48 h of incubation period. After two PBS washes, the cells were fixed overnight at −20 °C in 70% ethanol. Following fixation and washing AsPC-1 cells with PBS, they were stained for 30 min at room temperature, in the absence of light, using a DNA staining solution containing 20 $\mu\text{g/mL}$ PI and 200 $\mu\text{g/mL}$ RNase. Subsequently, analysis of a total of 20,000 events was performed using a FACS Calibur flow cytometer from BD Biosciences. CellQuest software (BD, USA) was used to determine the distribution of cells across sub-G1, G0/G1, S, and G2/M. Every experiment was repeated no fewer than three times.

Determination of apoptosis by Hoechst 33,258 staining

Hoechst 33,258 staining, employed as a DNA dye, was used to study apoptosis in AsPC-1 cells. Hoechst dyes attach to DNA molecules and produce fluorescence when exposed to ultraviolet (UV) light. AsPC-1 cells were initially seeded at a density of 15×10^4 cells/mL (2 mL per well) and incubated for 24 h in 6-well plates. After removing the media, the wells were treated with different concentration of **4a**, **4e**, and **4i** compounds, which were diluted in media, and then incubated for an additional 48 h. The media was removed, and one mL of the newly generated of 4% cold paraformaldehyde (PFA) was added, followed by a 20 min incubation. Afterward, the cells were washed twice with cold PBS and subsequently incubated with 1 mL of Hoechst 33,258 at a concentration of 2.5 μ g/mL for 30 min in the dark. Finally, the morphological alterations characteristic of apoptosis was evaluated using a fluorescence microscope (Nikon model DS-Ri2) after a final wash with PBS.

Statistics

One-way analysis of variance (ANOVA) was used for multiple comparisons, followed by Fisher's Least Significant Difference (LSD) test, performed with Statistical Package for the Social Sciences (SPSS) version 13 for Windows. Statistical significance was considered at $P < 0.05$.

Computational study

Molecular modeling analysis

The smina docking program aimed to explore the binding affinity and crucial molecular interactions between the target binding sites and the synthetic compounds⁶⁶. The crystal structures of CDK2/cyclin A, FLT4, and PDGFRA were obtained from RCSB-PDB website and EBI AlphaFold database and each protein was subsequently purified by removing any associated water molecules and co-crystal structures. AutoDock Tools 1.5.6 (ADT) (<https://mgltools/>) were allocated to further preparation of the protein by adding the hydrogens and assigning Kollmann charges. The Marvin sketch (<https://chemaxon.com/>) software was utilized to draw all the compounds, and HyperChem software⁶⁷ was employed to add hydrogen atoms. The synthetic compounds were optimized (gasteiger charge and energy) using the Open Babel⁶⁸. Subsequently, the smina software was employed to determine the interactions of the binding modes and minimize affinity within the binding site of the enzymes. To explore binding interactions, the Discovery Studio 2021 client (<https://discover.3ds.com/discovery-studio-visualizer>) was used.

Molecular dynamics simulation

The Gromacs dynamics package 2019.1, operating on a Centos Linux server with GPUs, was employed to conduct molecular modeling and dynamics simulations of the target compound (**4a**) in complex with CDK2, FLT4, and PDGFRA kinase. The MD simulation parameters were obtained by the Amber99sb force field to define at 300 K and neutral pH (7.0). Force field parameters were generated by ACPYPE software⁶⁹ and the AM1 partial charges were added by chimera software. A dodecahedral box surrounded the solute, which was then saturated by TIP3P water molecules with the addition of an adequate amount of Na^+ ions to neutralize the system. The steepest descent method was employed twice, with constraints and then without it, to minimize the energy of the system in the explicit solvent. Subsequently, NVT heating with V-rescale thermostats was executed, imposing restraints on the positions of the macromolecule and ligand atoms for a duration of 500 ps. Using the particle-mesh Ewald (PME) approaches and the LINCS constraint, which is faster than the SHAKE technique the periodic boundary conditions were examined. After the 500 ps equilibration phase in the NPT ensemble, the system's Pressure stabilized at 1 bar. The MD was run for 100 ns to achieve the best equilibration point. Following that, the trajectory was saved to account for any deviations in its path caused by the periodic boundary condition, and the complex was then repositioned at the center of the box. The root-mean-square deviation (RMSD) for protein backbone atoms, radius of gyration (R_g), and residue root-means-square fluctuation (RMSF) were analyzed in each snapshot against the primary frame. Also, the Gromos method was applied to cluster the trajectory in the equilibrium time range with cut-off values 0.14, 0.18, and 0.25 for CDK2/cyclin A, FLT4, and PDGFRA respectively. All binding interactions and generating images were analyzed by Discovery Studio Visualizer v20.1.0.19295.

Data availability

The PDBs codes (4BCQ and 6JOL) were retrieved from protein data bank (www.rcsb.org). <https://www.rcsb.org/structure/4BCQ> and [6jol](https://www.rcsb.org/structure/6JOL). The proteins crystal structure was downloaded from the AlphaFold database (<https://alphafold.ebi.ac.uk>) (UniProt code: P35916). The raw data used to generate figures and tables will be made available upon reasonable request.

Received: 20 July 2024; Accepted: 20 January 2025

Published online: 24 February 2025

References

- Sharma, P., Jhawar, V., Mathur, P. & Dutt, R. Innovation in cancer therapeutics and regulatory perspectives. *Medical Oncology* **39**, 76 (2022).
- Sung, H. *et al.* Global cancer statistics 2020: GLOBOCAN estimates of incidence and mortality worldwide for 36 cancers in 185 countries. *CA: a cancer journal for clinicians* **71**, 209–249 (2021).
- Abbas, Z. & Rehman, S. An overview of cancer treatment modalities. *Neoplasia* **1**, 139–157 (2018).
- Dembic, Z. Antitumor drugs and their targets. *Molecules* **25**, 5776 (2020).
- Roskoski Jr, R. A historical overview of protein kinases and their targeted small molecule inhibitors. *Pharmacological research* **100**, 1–23 (2015).

6. Kannaiyan, R. & Mahadevan, D. A comprehensive review of protein kinase inhibitors for cancer therapy. *Expert review of anticancer therapy* **18**, 1249–1270 (2018).
7. Garuti, L., Roberti, M. & Bottegoni, G. Multi-kinase inhibitors. *Current medicinal chemistry* **22**, 695–712 (2015).
8. Roskoski Jr, R. Sunitinib: a VEGF and PDGF receptor protein kinase and angiogenesis inhibitor. *Biochemical and biophysical research communications* **356**, 323–328 (2007).
9. Wilhelm, S. *et al.* Discovery and development of sorafenib: a multikinase inhibitor for treating cancer. *Nature reviews Drug discovery* **5**, 835–844 (2006).
10. Deininger, M., Buchdunger, E. & Druker, B. J. The development of imatinib as a therapeutic agent for chronic myeloid leukemia. *Blood* **105**, 2640–2653 (2005).
11. Alotaibi, A. A., Asiri, H. H., Rahman, A. M. & Alanazi, M. M. Novel pyrrolo [2, 3-d] pyrimidine derivatives as multi-kinase inhibitors with VEGFR-2 selectivity. *Journal of Saudi Chemical Society* **27**, 101712 (2023).
12. Liu, L. *et al.* Sorafenib blocks the RAF/MEK/ERK pathway, inhibits tumor angiogenesis, and induces tumor cell apoptosis in hepatocellular carcinoma model PLC/PRF/5. *Cancer research* **66**, 11851–11858 (2006).
13. Buchdunger, E., O'Reilly, T. & Wood, J. Pharmacology of imatinib (STI571). *European journal of cancer* **38**, S28–S36 (2002).
14. Ding, L. *et al.* The roles of cyclin-dependent kinases in cell-cycle progression and therapeutic strategies in human breast cancer. *International journal of molecular sciences* **21**, 1960 (2020).
15. Tadesse, S., Caldon, E. C., Tilley, W. & Wang, S. Cyclin-dependent kinase 2 inhibitors in cancer therapy: an update. *Journal of medicinal chemistry* **62**, 4233–4251 (2018).
16. Pang, W., Li, Y., Guo, W. & Shen, H. Cyclin E: a potential treatment target to reverse cancer chemoresistance by regulating the cell cycle. *American Journal of Translational Research* **12**, 5170 (2020).
17. Hume, S., Dianov, G. L. & Ramadan, K. A unified model for the G1/S cell cycle transition. *Nucleic acids research* **48**, 12483–12501 (2020).
18. Peyressat, M., Prével, C., Pellerano, M. & Morris, M. C. Targeting cyclin-dependent kinases in human cancers: from small molecules to peptide inhibitors. *Cancers* **7**, 179–237 (2015).
19. Martin, M. P., Olesen, S. H., Georg, G. I. & Schönbrunn, E. Cyclin-dependent kinase inhibitor dinaciclib interacts with the acetyl-lysine recognition site of bromodomains. *ACS chemical biology* **8**, 2360–2365 (2013).
20. Kuchukulla, R. R. *et al.* Novel 2, 6, 9-trisubstituted purines as potent CDK inhibitors alleviating trastuzumab-resistance of HER2-positive breast cancers. *Pharmaceuticals* **15**, 1041 (2022).
21. El-Moghazy, S. M., Ibrahim, D. A., Abdelgawad, N. M., Farag, N. A. & El-Khouly, A. S. Design, synthesis and biological evaluation of novel pyrimido [4, 5-d] pyrimidine CDK2 Inhibitors as anti-tumor agents. *Scientia Pharmaceutica* **79**, 429–448 (2011).
22. Alexander, L. T. *et al.* Type II inhibitors targeting CDK2. *ACS chemical biology* **10**, 2116–2125 (2015).
23. Wang, Y. *et al.* Design, synthesis and biological evaluation of pyrimidine derivatives as novel CDK2 inhibitors that induce apoptosis and cell cycle arrest in breast cancer cells. *Bioorganic & medicinal chemistry* **26**, 3491–3501 (2018).
24. Williamson, D. S. *et al.* Structure-guided design of pyrazolo [1, 5-a] pyrimidines as inhibitors of human cyclin-dependent kinase 2. *Bioorganic & medicinal chemistry letters* **15**, 863–867 (2005).
25. Li, K. *et al.* Target ROS to induce apoptosis and cell cycle arrest by 5, 7-dimethoxy-1, 4-naphthoquinone derivative. *Bioorganic & Medicinal Chemistry Letters* **28**, 273–277 (2018).
26. Manickam, M. *et al.* Investigation of chemical reactivity of 2-alkoxy-1, 4-naphthoquinones and their anticancer activity. *Bioorganic & Medicinal Chemistry Letters* **28**, 2023–2028 (2018).
27. Qiu, H. Y. *et al.* Naphthoquinones: A continuing source for discovery of therapeutic antineoplastic agents. *Chemical biology & drug design* **91**, 681–690 (2018).
28. Sohail, M., Sun, Z., Li, Y., Gu, X. & Xu, H. Research progress in strategies to improve the efficacy and safety of doxorubicin for cancer chemotherapy. *Expert review of anticancer therapy* **21**, 1385–1398 (2021).
29. Lankelma, J. *et al.* Doxorubicin gradients in human breast cancer. *Clinical cancer research* **5**, 1703–1707 (1999).
30. Poirier, T. I. Mitoxantrone. *Drug intelligence & clinical pharmacy* **20**, 97–105 (1986).
31. Gholampour, M. *et al.* Click chemistry-assisted synthesis of novel aminonaphthoquinone-1, 2, 3-triazole hybrids and investigation of their cytotoxicity and cancer cell cycle alterations. *Bioorganic Chemistry* **88**, 102967 (2019).
32. Alam, M. M. 1, 2, 3-Triazole hybrids as anticancer agents: a review. *Archiv der Pharmazie* **355**, 2100158 (2022).
33. Bahia, S. B. B. *et al.* Molecular hybridization as a powerful tool towards multitarget quinoidal systems: Synthesis, trypanocidal and antitumor activities of naphthoquinone-based 5-iodo-1, 4-disubstituted-, 1, 4-and 1, 5-disubstituted-1, 2, 3-triazoles. *MedChemComm* **7**, 1555–1563 (2016).
34. Ravichandiran, P. *et al.* Synthesis and anticancer evaluation of 1, 4-naphthoquinone derivatives containing a phenylaminosulfonyl moiety. *ChemMedChem* **14**, 532–544 (2019).
35. Angulo-Elizari, E., Henriquez-Figueroa, A., Morán-Serradilla, C., Plano, D. & Sanmartín, C. Unlocking the potential of 1, 4-naphthoquinones: A comprehensive review of their anticancer properties. *European Journal of Medicinal Chemistry*, 116249 (2024).
36. Valença, W. O. *et al.* Synthesis of quinone-based N-sulfonyl-1, 2, 3-triazoles: chemical reactivity of Rh (II) azavinyl carbenes and antitumor activity. *ChemistrySelect* **2**, 4301–4308 (2017).
37. Prasad, C. V., Nayak, V. L., Ramakrishna, S. & Mallavadhani, U. V. Novel menadione hybrids: Synthesis, anticancer activity, and cell-based studies. *Chemical Biology & Drug Design* **91**, 220–233 (2018).
38. Chipoline, I. C. *et al.* Molecular mechanism of action of new 1, 4-naphthoquinones tethered to 1, 2, 3-1H-triazoles with cytotoxic and selective effect against oral squamous cell carcinoma. *Bioorganic Chemistry* **101**, 103984 (2020).
39. Wang, H. *et al.* Recent Progress in CDK4/6 Inhibitors and PROTACs. *Molecules* **28**, 8060 (2023).
40. Li, Y. *et al.* Discovery, synthesis, and evaluation of highly selective vascular endothelial growth factor receptor 3 (VEGFR3) inhibitor for the potential treatment of metastatic triple-negative breast cancer. *Journal of Medicinal Chemistry* **64**, 12022–12048 (2021).
41. Roth, G. J. *et al.* Nintedanib: from discovery to the clinic. *Journal of medicinal chemistry* **58**, 1053–1063 (2015).
42. Jumper, J. *et al.* Highly accurate protein structure prediction with AlphaFold. *Nature* **596**, 583–589 (2021).
43. Schneider, S. *et al.* Resequencing of VEGFR3 pathway genes implicate GJC2 and FLT4 in the formation of primary congenital chylothorax. *American journal of medical genetics. Part A* **188**, 1607–1611 (2022).
44. Daina, A., Michielin, O. & Zoete, V. SwissADME: a free web tool to evaluate pharmacokinetics, drug-likeness and medicinal chemistry friendliness of small molecules. *Scientific reports* **7**, 42717 (2017).
45. Al-Sanea, M. M. *et al.* A new CDK2 inhibitor with 3-hydrazonoinodol-2-one scaffold endowed with anti-breast cancer activity: Design, synthesis, biological evaluation, and in silico insights. *Molecules* **26**, 412 (2021).
46. Meng, X. *et al.* Erdaftinib inhibits tumorigenesis of human lung adenocarcinoma A549 by inducing S-phase cell-cycle arrest as a CDK2 inhibitor. *Molecules* **27**, 6733 (2022).
47. Barakat, A. *et al.* New spiro-indeno [1, 2-b] quinoxalines clubbed with benzimidazole scaffold as CDK2 inhibitors for halting non-small cell lung cancer; stereoselective synthesis, molecular dynamics and structural insights. *Journal of Enzyme Inhibition and Medicinal Chemistry* **38**, 2281260 (2023).
48. Lim, T.-G. *et al.* Curcumin suppresses proliferation of colon cancer cells by targeting CDK2. *Cancer Prevention Research* **7**, 466–474 (2014).
49. Huang, J. *et al.* CDK1/2/5 inhibition overcomes IFNG-mediated adaptive immune resistance in pancreatic cancer. *Gut* **70**, 890–899 (2021).

50. Hsu, M.-C., Pan, M.-R. & Hung, W.-C. Two birds, one stone: double hits on tumor growth and lymphangiogenesis by targeting vascular endothelial growth factor receptor 3. *Cells* **8**, 270 (2019).
51. Walsh, K. A. *et al.* SAR131675, a VEGFR3 Inhibitor, Modulates the Immune Response and Reduces the Growth of Colorectal Cancer Liver Metastasis. *Cancers* **14**, 2715 (2022).
52. Zou, X. *et al.* Targeting the PDGF/PDGFR signaling pathway for cancer therapy: A review. *International Journal of Biological Macromolecules* **202**, 539–557 (2022).
53. Papadopoulos, N. & Lennartsson, J. The PDGF/PDGFR pathway as a drug target. *Molecular aspects of medicine* **62**, 75–88 (2018).
54. Viola, D., Cappagli, V. & Elisei, R. Cabozantinib (XL184) for the treatment of locally advanced or metastatic progressive medullary thyroid cancer. *Future oncology* **9**, 1083–1092 (2013).
55. Gossage, L. & Eisen, T. Targeting multiple kinase pathways: a change in paradigm. *Clinical Cancer Research* **16**, 1973–1978 (2010).
56. D'Costa, M. *et al.* CDK regulators—Cell cycle progression or apoptosis—Scenarios in normal cells and cancerous cells. *Advances in Protein Chemistry and Structural Biology* **135**, 125–177 (2023).
57. Noble, M. E., Endicott, J. A. & Johnson, L. N. Protein kinase inhibitors: insights into drug design from structure. *Science* **303**, 1800–1805 (2004).
58. Hassan, G. S., Rahman, D. E. A., Nissan, Y. M., Abdelmajeed, E. A. & Abdelghany, T. M. Novel pyrazolopyrimidines: Synthesis, in vitro cytotoxic activity and mechanistic investigation. *European Journal of Medicinal Chemistry* **138**, 565–576 (2017).
59. Pai, A. & BS, J. Novel benzylidene benzofuranone analogues as potential anticancer agents: design, synthesis and in vitro evaluation based on CDK2 inhibition assays. *3 Biotech* **12**, 256 (2022).
60. Chamduang, C. *et al.* Novel triazole-tetrahydroisoquinoline hybrids as human aromatase inhibitors. *Bioorganic Chemistry* **93**, 103327 (2019).
61. Damghani, T. *et al.* Imidazopyridine hydrazone derivatives exert antiproliferative effect on lung and pancreatic cancer cells and potentially inhibit receptor tyrosine kinases including c-Met. *Scientific Reports* **11**, 3644 (2021).
62. Ben-David, I., Rozen, Y., Ortu, G. & Mishani, E. Radiosynthesis of ML03, a novel positron emission tomography biomarker for targeting epidermal growth factor receptor via the labeling synthon:[11 C] acryloyl chloride. *Applied radiation and isotopes* **58**, 209–217 (2003).
63. Divar, M. *et al.* Novel spiroindoline quinazolinone derivatives as anticancer agents and potential FLT3 kinase inhibitors. *Bioorganic & medicinal chemistry* **90**, 117367, doi:10.1016/j.bmc.2023.117367 (2023).
64. Mortazavi, M. *et al.* Novel quinazoline-1,2,3-triazole hybrids with anticancer and MET kinase targeting properties. *Sci Rep* **13**, 14685, doi:10.1038/s41598-023-41283-2 (2023).
65. Moosavi, F. *et al.* Antiproliferative effect, alteration of cancer cell cycle progression and potential MET kinase inhibition induced by 3, 4-dihydropyrimidin-2 (1H)-one C5 amide derivatives. *European Journal of Pharmacology* **894**, 173850 (2021).
66. Koes, D. R., Baumgartner, M. P. & Camacho, C. J. Lessons learned in empirical scoring with smina from the CSAR 2011 benchmarking exercise. *Journal of chemical information and modeling* **53**, 1893–1904 (2013).
67. Laxmi, D. & Priyadarshy, S. HyperChem 6.03. *Biotech Software & Internet Report: The Computer Software Journal for Scientists* **3**, 5–9 (2002).
68. O'Boyle, N. M. *et al.* Open Babel: An open chemical toolbox. *Journal of cheminformatics* **3**, 1–14 (2011).
69. Sousa da Silva, A. W. & Vranken, W. F. ACPYPE-Antechamber python parser interface. *BMC research notes* **5**, 1–8 (2012).

Acknowledgements

The authors are thankful to the Vice-Chancellor for Research, Shiraz University of Medical Sciences for the financial support of this work (Grant number: 30915). This study was part of the PhD thesis project of Pegah Mardaneh (Grant number: 23234).

Author contributions

P.M. synthesized compounds, performed the biological assay, performed molecular modeling study, Wrote - original draft & editing. S.P. Contributed to molecular modeling study and editing the manuscript. M.M. Contributed to the biological section. M.Kh. Contributed and supervised the design and characterization of compounds as well as the preparation of the manuscript. Z.R. Contributed to the preparation and editing of the manuscript. L.S. Funding acquisition and wrote- review & editing. N.E. Contributed and supervised the design and characterization of compounds as well as the preparation of the manuscript. O.F. Contributed and supervised the design and characterization of the biological assay as well as the preparation of the manuscript.

Declarations

Ethics approval and consent to participate

Not applicable.

Consent for publication

Not applicable.

Competing interests

The authors declare no competing interests.

Additional information

Supplementary Information The online version contains supplementary material available at <https://doi.org/10.1038/s41598-025-87483-w>.

Correspondence and requests for materials should be addressed to N.E. or O.F.

Reprints and permissions information is available at www.nature.com/reprints.

Publisher's note Springer Nature remains neutral with regard to jurisdictional claims in published maps and institutional affiliations.

Open Access This article is licensed under a Creative Commons Attribution-NonCommercial-NoDerivatives 4.0 International License, which permits any non-commercial use, sharing, distribution and reproduction in any medium or format, as long as you give appropriate credit to the original author(s) and the source, provide a link to the Creative Commons licence, and indicate if you modified the licensed material. You do not have permission under this licence to share adapted material derived from this article or parts of it. The images or other third party material in this article are included in the article's Creative Commons licence, unless indicated otherwise in a credit line to the material. If material is not included in the article's Creative Commons licence and your intended use is not permitted by statutory regulation or exceeds the permitted use, you will need to obtain permission directly from the copyright holder. To view a copy of this licence, visit <http://creativecommons.org/licenses/by-nc-nd/4.0/>.

© The Author(s) 2025